RSC Applied Interfaces

ROYAL SOCIETY OF CHEMISTRY

REVIEW

View Article Online
View Journal

Cite this: DOI: 10.1039/d6lf00024j

Materials design strategies for semiconducting metal-oxide chemiresistive gas sensors: a review

Maosong Tian,[a] Yufan Wu,[a] Zhihao Zhao,[a] Zhe Chen,[a] Nansong Zhu[b] and Xiangyu Jiang *[ac]

Semiconducting metal-oxide (SMO) chemiresistive gas sensors have been extensively investigated owing to their simple device architecture, high sensitivity, and compatibility with large-scale fabrication. Despite substantial progress, further performance improvement remains strongly constrained by intrinsic sensing mechanisms, particularly under complex gas backgrounds and humid environments. This review focuses on representative material design strategies that have demonstrated clear mechanism–performance correlations in SMO-based chemiresistive sensors. We critically discuss the underlying sensing mechanisms associated with heterojunction engineering, defect and phase control, metal catalysts, gas filtration, and microstructure design, highlighting both their performance advantages and inherent limitations. Finally, current challenges related to these limitations are summarized, and future development directions toward application-oriented SMO gas sensors are discussed. This review aims to offer valuable insights and inspiration for designing SMO resistive gas sensors, thereby advancing gas sensing performance.

Received 27th January 2026,
Accepted 24th February 2026

DOI: 10.1039/d6lf00024j

rsc.li/RSCApplInter

1. Introduction

The increasing demand for real-time monitoring of hazardous and pollutant gases has driven rapid development of portable and low-cost gas sensing technologies.[1–4] In this context, chemiresistive sensors remain one of the most widely studied platforms due to their simple signal transduction, compatibility with microfabrication, and potential for large-scale deployment.[5–9] The performance of chemiresistors is intrinsically governed by the properties of their sensing materials. Thus, a wide range of materials have been explored, including conducting polymers,[10–12] porous frameworks,[13–15] two-dimensional materials,[16,17] and semiconducting metal oxides.[18–21] While each class exhibits distinct advantages, such as room-temperature operation for polymers or molecular selectivity in porous frameworks, semiconducting metal oxides (SMOs) remain the most extensively investigated owing to their tunable surface chemistry, thermal robustness, and stable electrical characteristics.[22–24]

Despite significant advances in material synthesis and device engineering, the sensing performance of SMO chemiresistors is still fundamentally limited by their mechanism of operation.[25] Gas detection relies on surface redox reactions involving adsorbed oxygen species, which inherently leads to poor chemical specificity and pronounced cross-sensitivity, particularly in humid or multicomponent environments.[26,27] Although extensive reviews have analyzed sensing mechanisms, material selection, morphological effects, and selectivity strategies independently, fewer works explicitly map engineering strategies onto the fundamental sensing processes they perturb. Therefore, it is necessary to establish a mechanism–performance mapping framework that clarifies how distinct engineering approaches influence adsorption thermodynamics, reaction kinetics, charge transport, and signal formation.

Herein, this review summarizes recent progress in SMO-based chemiresistive gas sensors from a mechanism-oriented perspective. We introduce the fundamental sensing principles and typical device configurations, followed by a systematic discussion of key performance enhancement strategies, including heterojunction engineering, defect and phase control, metal catalysts, gas filtration, and microstructure design. By distinguishing between signal amplification and pathway modification, we aim to provide a mechanistic context for evaluating the potential and limitations of current materials design strategies.

2. Structure and mechanisms of SMO chemiresistive gas sensors

Fig. 1a illustrates a typical configuration of a chemiresistive gas sensor based on SMOs. The sensing behavior of

[a] School of Chemistry, Beihang University, Beijing 100191, China.
E-mail: jiangxy@buaa.edu.cn
[b] Department of Chemistry, National Demonstration Centre for Experimental Chemistry Education, College of Science, Yanbian University, Yanji, 133002, PR China
[c] International Research Institute for Multidisciplinary Science, Beihang University, Beijing 100191, China

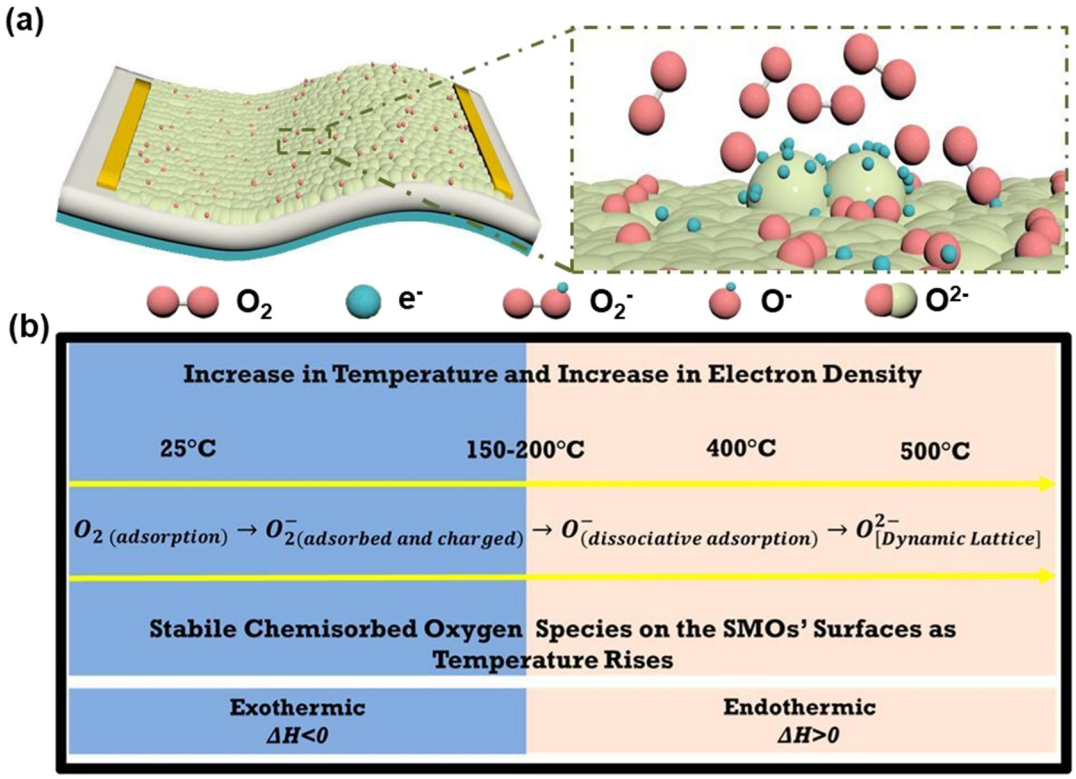

Fig. 1 (a) A typical configuration of a chemiresistive gas sensor based on SMOs. (b) Transformation and stability of oxygen ions as temperature rises on SMOs surfaces. Reproduced with permission.[35] Copyright 2023, Ciftyurek *et al.*

chemiresistive gas sensors based on SMOs originates from the coupling between surface chemical reactions and near-surface charge transport. Rather than reflecting a purely bulk property, the measured resistance is primarily governed by surface band bending and the modulation of space-charge regions induced by gas–solid interactions. Under ambient conditions, oxygen molecules are adsorbed on the SMO surface and extract electrons from the semiconductor, forming chemisorbed oxygen species (typically O_2^-, O^-, and O^{2-}). This electron-withdrawing process induces upward band bending near the surface of n-type SMOs, leading to the formation of an electron depletion layer and an increased baseline resistance. In p-type SMOs, the same oxygen adsorption process effectively increases the surface hole concentration, resulting in a hole accumulation layer and a relatively lower resistance in air.[28–30]

Upon exposure to reducing gases, surface redox reactions occur between the target molecules and the chemisorbed oxygen species. These reactions consume surface oxygen and release the trapped electrons back to the semiconductor. For n-type SMOs, the returned electrons narrow the depletion layer and lower the surface potential barrier, thereby facilitating electron transport and decreasing the sensor resistance. In contrast, in p-type SMOs, the injected electrons recombine with holes in the accumulation layer, suppressing hole conduction and increasing the interfacial barrier for hole transport, which manifests as an increase in resistance. Although n-type and p-type SMOs exhibit opposite resistance trends toward reducing gases, both responses stem from the same fundamental process: modulation of surface band structure and charge-carrier distribution by gas-induced redox reactions.[31–33] Table 1 summarizes the changes in electrical resistance of different SMOs exposed to oxidizing and reducing gases.

The chemical identity and reactivity of surface oxygen species play a central role in governing sensing performance. Oxygen molecules (O_2) adsorbed on the surface of metal oxide semiconductors capture free electrons from the conduction band of the sensing layer according to the following equilibria:[35,36]

Molecularly adsorbed superoxide: O_2 (ads) + e^- ⇌ O_2^- (ads)

Chemisorbed atomic oxygen: O_2^- (ads) + e^- ⇌ $2O^-$ (ads)

Lattice-related oxygen: O^- (ads) + e^- ⇌ O^{2-} (ads)

The dominant oxygen species is strongly dependent on operating temperature (Fig. 1b). At relatively low temperatures, oxygen is preferentially adsorbed in a molecular form as

Table 1 Gas sensing behaviors of SMOs in different gases[34]

Conduction types	Reducing gas	Oxidizing gas
n-type	Resistance decrease	Resistance increase
p-type	Resistance increase	Resistance decrease

superoxide species (O_2^-), since limited thermal energy and sluggish surface kinetics hinder dissociative adsorption. They are mainly adsorbed on the semiconductor surface in molecular form and capture one electron from the conduction band to form O_2^-. These species exhibit relatively low chemical reactivity, leading to slow response and limited sensitivity. At intermediate temperatures, atomic oxygen species (O^-) become increasingly important and undergo a transition toward dissociative or strongly chemisorbed oxygen species, resulting in enhanced sensitivity and faster response times. At elevated temperatures, lattice-related oxygen species may participate in surface reactions, although the specific transition ranges vary significantly among different SMO materials and morphologies.[37] Excessively high temperatures may further induce direct combustion of analyte gases or accelerate structural degradation of the sensing layer, imposing practical constraints on sensor operation.[38–40] The creation and annihilation of oxygen vacancies modify local non-stoichiometry, alter charge-carrier concentration, and dynamically reshape the surface electronic structure. As a result, gas sensing in many SMOs cannot be fully described by surface adsorption alone, but rather involves coupled surface-lattice processes that evolve during operation.[41,42]

Humidity introduces an additional level of complexity to SMO-based gas sensing.[43] Most SMOs possess intrinsically hydrophilic surfaces, enabling competitive adsorption of water molecules alongside oxygen and target gases. Water adsorption can reduce the coverage of reactive oxygen species, introduce hydroxyl groups, and donate electrons to the surface, thereby altering baseline resistance and suppressing effective sensing reactions.[44] Importantly, humidity does not merely act as an external interferent but can fundamentally modify surface reaction pathways and charge-transport behavior. This mechanism-level interference represents one of the major challenges for achieving stable and selective gas detection under realistic operating conditions.[45]

3. General strategies for overcoming current limitations of SMO chemiresistive gas sensors

Over the past decade, a wide range of material design strategies have been proposed to mitigate these limitations (Fig. 2). Rather than functioning independently, these strategies can be understood as targeting a limited number of key physicochemical processes that govern chemiresistive sensing.[46] From a mechanism-oriented perspective, most performance-enhancement approaches can be broadly categorized according to how they regulate charge transport, surface reaction chemistry, mass transport, and reaction pathways. Establishing such a framework is essential for rationalizing the diverse strategies reported in the literature and for guiding future material design.

One major class of strategies focuses on modulating charge transport and interfacial barriers. By constructing

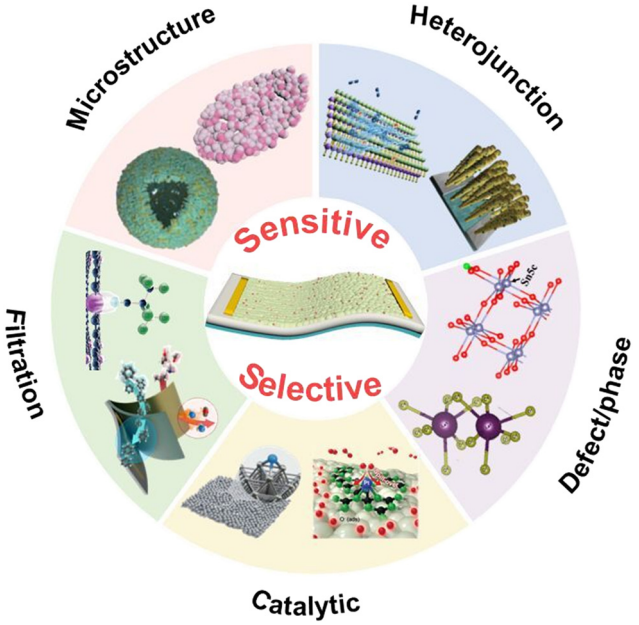

Fig. 2 Modification strategies for semiconducting metal-oxide resistive sensors. Reproduced with permission.[50] Copyright 2016, American Chemical Society. Reproduced with permission.[51] Copyright 2024, copyright 2016, American Chemical Society. Reproduced with permission.[52] Copyright 2016, American Chemical Society. Reproduced with permission.[53] Copyright 2025, Wiley-VCH. Reproduced with permission.[54] Copyright 2020, American Chemical Society. Reproduced with permission.[55] Copyright 2022, Wiley-VCH. Reproduced with permission.[56] Copyright 2023, Jeong *et al.* Reproduced with permission.[57] Copyright 2025, Wiley-VCH. Reproduced with permission.[58] Copyright 2022, Elsevier. Reproduced with permission.[59] Copyright 2019, Wiley-VCH.

heterojunctions between materials with different work functions, carrier types, or electronic structures, local band bending and space-charge regions can be deliberately engineered. The resulting built-in electric fields and interfacial barriers amplify resistance modulation upon gas exposure, enabling enhanced sensitivity and, in some cases, improved selectivity.[47–49] Heterojunction engineering therefore primarily addresses the limited modulation depth of pristine SMOs by strengthening the coupling between surface reactions and electrical transduction.

A second group of approaches aims to regulate surface chemistry and electronic structure through defect and phase control. Introducing oxygen vacancies, metal vacancies alter local charge-carrier concentration, adsorption energetics, and oxygen activation behavior. Similarly, controlling crystal phase, exposed facets, or polymorphism reshapes surface atomic configurations and reaction pathways.[60,61] These strategies directly influence the density and reactivity of surface active sites, thereby tuning both sensitivity and selectivity.[62] However, they also introduce challenges related to defect stability, phase evolution, and long-term reproducibility, highlighting the need for balanced and controllable design.

Catalysts, particularly through noble metal catalysts, represents a third important strategy that targets reaction

kinetics and pathway selectivity. Noble metal nanoparticles, clusters, or single atoms can lower activation barriers for gas adsorption, dissociation, and oxidation, accelerating surface redox reactions and enabling operation at reduced temperatures. At the same time, metal-oxide interfaces introduce additional electronic sensitization effects through Schottky barriers or localized charge transfer.[63] While catalytic strategies are highly effective in enhancing sensitivity and response speed, they often face issues such as catalyst poisoning, aggregation, and limited durability under harsh operating conditions.

In contrast to strategies that primarily modify the sensing material itself, gas filtration introduces an additional degree of freedom by controlling gas flux and reaction pathways prior to sensing. Sorption-based filters, molecular sieves, and catalytic filter layers selectively suppress interfering species or pre-convert gases into more detectable intermediates. By decoupling gas discrimination from the intrinsic response of the sensing layer, filtration strategies offer a powerful route to improving selectivity in complex environments.[64,65] However, their effectiveness is closely tied to humidity tolerance, regeneration capability, and compatibility with sensor operating conditions.

Finally, nanostructure design provides a structural platform that synergistically supports the aforementioned strategies by optimizing mass transport and surface exposure. 0–3D architectures influence gas diffusion kinetics, active-site accessibility, and charge-transport pathways. Hierarchical porous structures, in particular, can simultaneously enhance sensitivity, response speed, and stability by balancing surface area with efficient gas transport.[66,67] Nevertheless, excessive structural complexity or dense packing may hinder diffusion and compromise reproducibility, underscoring the importance of rational architectural design.

Taken together, these strategies as complementary tools that address different aspects of the sensing mechanism. Effective sensor design increasingly relies on the synergistic integration of multiple strategies, such as combining heterojunction-induced barrier modulation with catalytic activation and filtration-assisted selectivity. In the following sections, each strategy is discussed in detail, with emphasis on its underlying mechanism, advantages, limitations, and role within an integrated design framework for next-generation SMO chemiresistive gas sensors.

3.1 Heterojunction engineering

Heterojunction engineering represents one of the most widely adopted strategies for enhancing the performance of SMO chemiresistive gas sensors. From a mechanism-oriented perspective, the primary function of a heterojunction is not merely the formation of a built-in electric field, but rather the deliberate introduction of interfacial barriers whose height and width are highly sensitive to surface chemical reactions. This interfacial sensitivity enables small variations in surface charge states to be translated into amplified resistance changes.

3.1.1 p–n heterojunctions. Among various heterojunction configurations, p–n heterojunctions have been most extensively investigated due to their pronounced interfacial band bending and strong barrier effects. In p–n heterostructures composed of p-type and n-type SMOs, the Fermi level of the p-type material lies closer to the valence band maximum, whereas that of the n-type material resides near the conduction band minimum.[68] Consequently, the Fermi level of the n-type semiconductor is higher than that of the p-type semiconductor. This intrinsic difference in Fermi-level positions provides the thermodynamic driving force for charge redistribution once the two phases are joined. Upon contact, electrons spontaneously diffuse from the n-type region into the p-type region, while holes diffuse in the opposite direction. This bidirectional carrier migration proceeds until the Fermi levels align across the interface, resulting in electronic equilibrium.[69] During this process, electrons leaving the n-type side create a positively charged donor-ionized region, while hole outflow from the p-type side leads to a negatively charged acceptor-ionized region. These oppositely charged layers form a well-defined space-charge region, within which a depletion layer develops and a built-in potential barrier is constructed.[70] For reference, Table 2 listed some sensing materials with their respective conduction types.

When exposed to target analytes, oxygen species pre-adsorbed on the surface of the heterostructure participate in redox reactions with gas molecules, releasing electrons back into the semiconductor. The injected electrons partially compensate the interfacial ionized charges, thereby narrowing the depletion region and lowering the potential barrier height. Even a subtle modulation of the barrier width or height can result in significant variations in charge-carrier mobility across the junction, producing a pronounced change in overall resistance. This barrier-controlled transport mechanism is the fundamental reason why p–n heterojunctions often exhibit amplified sensing responses, faster reaction kinetics, and higher sensitivity compared with their single-phase counterparts.[74]

During the construction of heterostructures, the morphology and interfacial chemical environment of the materials also play crucial roles in determining gas selectivity. Xu *et al.*[75] significantly enhanced both the selectivity and sensitivity of their sensor toward formaldehyde by engineering the heterojunction interface between n-type SnO_2 and p-type NiO (Fig. 3a). The formation of the heterojunction induced energy band bending at the interface and redistribution of charge carriers, resulting in a thicker electron depletion layer on the SnO_2 surface. In air, the sensor exhibited a high-resistance state. When exposed to the reducing gas formaldehyde, the surface reactions released electrons back into the conduction band, narrowing the

Table 2 Conduction types of SMOs[71–73]

Conduction types	SMO materials
n	SnO_2, ZnO, TiO_2, Al_2O_3, In_2O_3, V_2O_5, α-Fe_2O_3, CeO_2
p	NiO, CuO, Co_3O_4, Cr_2O_3, Mn_3O_4, $LaFeO_3$, PdO, Y_2O_3

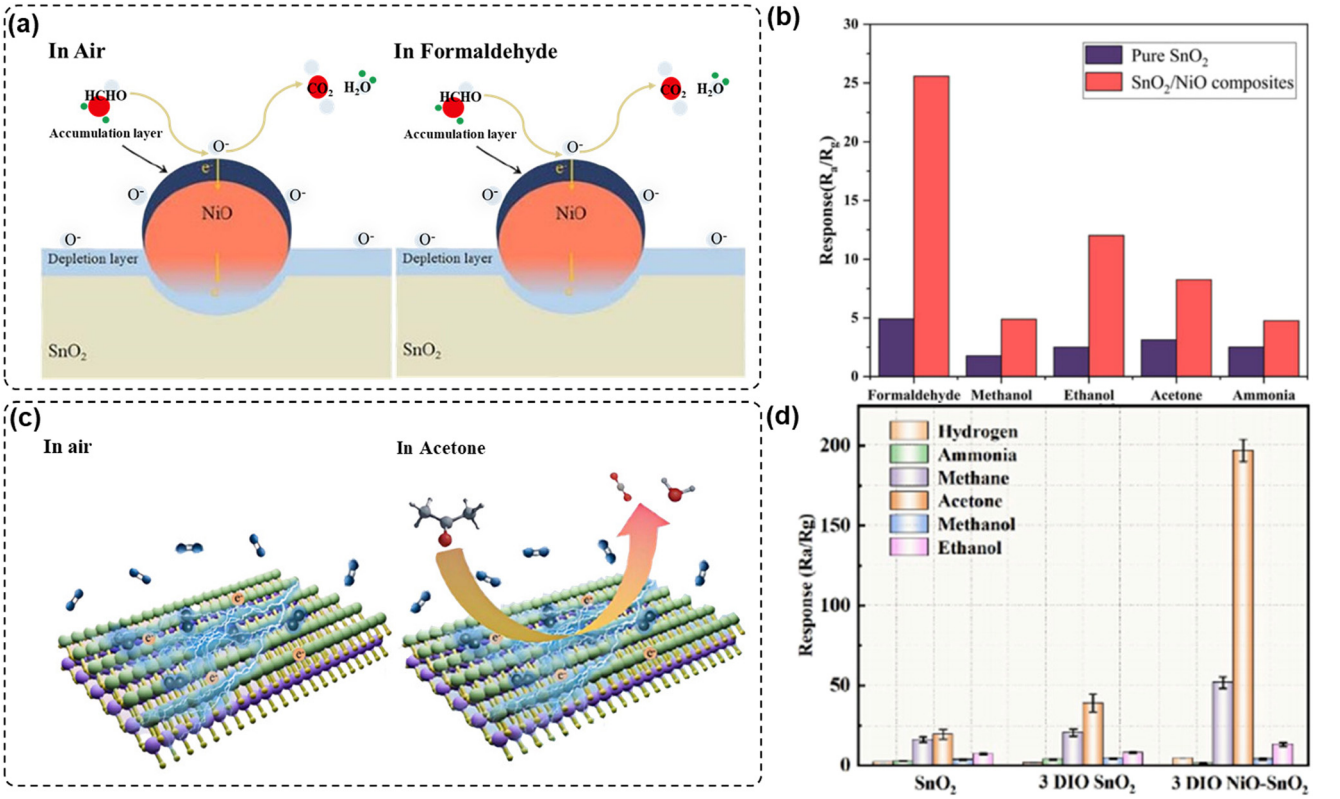

Fig. 3 (a) Schematic diagrams depicting the depletion layer and potential barrier-forming at the SnO_2/NiO junction upon exposure to air and formaldehyde. (b) Response of samples to 250 ppm of different gases at 230 °C. Reproduced with permission.[75] Copyright 2020, The Materials Research Society. (c) Sensing mechanism of the three-dimensional inverse opal macroporous SnO_2 doped with NiO sensor in air and acetone. (d) Selectivity tests of the three sensors to 100 ppm different gases. Reproduced with permission.[50] Copyright 2025, American Chemical Society.

depletion layer and lowering the potential barrier, which in turn decreased the resistance and produced a strong response signal. In addition, the introduction of NiO not only facilitated oxygen adsorption and activation but also reduced the activation energy of the formaldehyde oxidation reaction through its catalytic effect, further improving both response speed. Structural characterization confirmed that the amount of adsorbed oxygen increased markedly in the SnO_2/NiO heterojunction, effectively regulating its selectively of formaldehyde (Fig. 3b).

Differently from Xu and coauthors, Li *et al.*[50] fabricated a three-dimensional inverse opal macroporous SnO_2/NiO heterojunction by uniformly doping NiO into SnO_2 (Fig. 3c). Because the work function of NiO is higher than that of SnO_2, electrons diffused from SnO_2 to NiO upon contact, placing the material in a high-resistance state in air. Notably, the three-dimensional inverse opal architecture, with its large specific surface area and ordered macroporous channels, promoted acetone diffusion and provided abundant active sites for gas reactions. The sensor exhibited selective for acetone, achieving a response value of up to 202% at 198.5 °C with a response time of only 3 s (Fig. 3d).

It should be noted that the sensing enhancement in p–n heterojunctions cannot always be attributed solely to band-structure effects. In many reported systems, catalytic activity, altered oxygen adsorption behavior, and increased surface defect density at the heterointerface also contribute substantially to the observed performance. Disentangling these coupled effects remains a challenge and requires careful experimental design and mechanistic analysis.

3.1.2 p–p and n–n heterojunctions. In contrast to p–n junctions, isotype heterojunctions formed between two n-type or two p-type semiconductors do not exhibit rectifying behavior, yet they can still significantly influence sensing performance. In n–n heterojunctions, differences in Fermi level position and carrier concentration lead to asymmetric band bending, resulting in the formation of electron accumulation and depletion regions on opposite sides of the interface. The associated potential barrier can impede carrier transport in one direction while facilitating it in the other, rendering the overall resistance sensitive to surface charge modulation.[76]

In a typical n–n heterojunction, performance enhancement is achieved through the mismatch in work function or carrier density. Zhu *et al.*[77] constructed an n–n heterojunction material by loading WO_3 onto In_2O_3 micro-rods (Fig. 4a). This structure exhibits a response value of 678.4 to 20 ppm triethylamine at 160 °C, with a response time of only 11 seconds and a detection limit as low as 0.08 ppm (Fig. 4b), along with excellent selectivity (Fig. 4c). The enhanced performance can be attributed to three key factors:

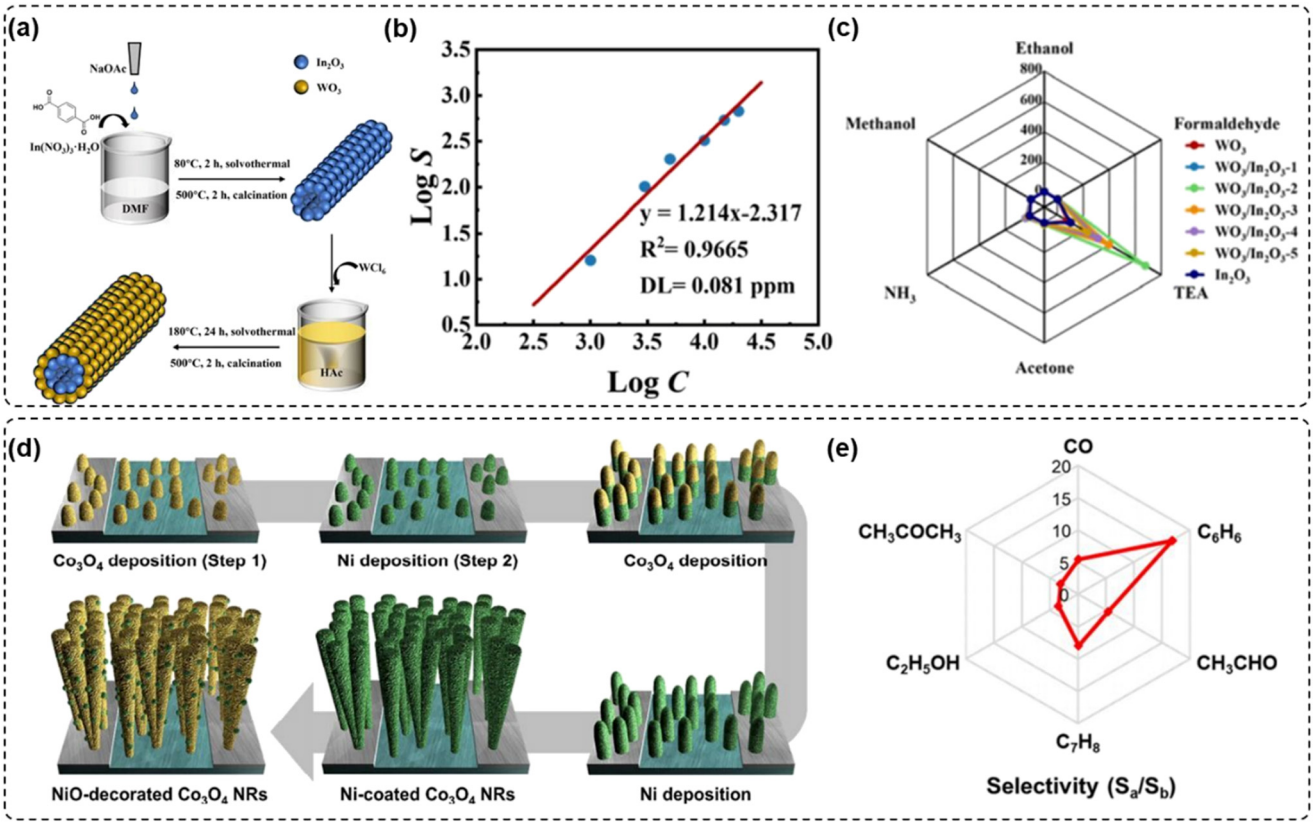

Fig. 4 (a) The schematic diagram of synthesis of the WO_3/In_2O_3. (b) The linear relationship of log *S*–log *C* plots to triethylamine. (c) The response toward different gases of all sensors measured at 160 °C. Reproduced with permission.[77] Copyright 2025, Royal Society of Chemistry. (d) Fabrication procedure of NiO-decorated Co_3O_4 nanorods. (e) Selectivity of NiO-decorated Co_3O_4 nanorods to various gases (50 ppm) at 350 °C. Reproduced with permission.[51] Copyright 2024, Elsevier.

the electron depletion layer formed at the heterojunction interface improves charge separation efficiency; the hierarchical structure of the material provides a high specific surface area and abundant gas diffusion channels; the specific adsorption of triethylamine molecules by WO_3 and the synergistic catalytic effect of In_2O_3 together promote the gas–solid interface reaction.

Similarly, p–p heterojunctions introduce interfacial barriers for hole transport through redistribution of hole concentration across the interface. Although the modulation depth of these barriers is generally smaller than that of p–n junctions, p–p heterostructures can still enhance sensing performance, particularly for p-type SMOs that otherwise suffer from limited carrier mobility and weak resistance modulation. In such systems, heterojunction formation effectively amplifies the influence of surface reactions on hole transport.[78]

The design concept of p–p heterojunctions is to introduce an additional interfacial hole barrier, thereby enhancing the sensitivity of p-type sensing materials. For instance, Suh *et al.*[51] fabricated vertically aligned Co_3O_4 nanorods using a multi-step glancing-angle deposition method and subsequently deposited Ni onto their surface. After annealing, the Ni was converted into NiO nanoparticles, forming a p–p heterojunction (Fig. 4d). This structure delivered a response to 50 ppm benzene that was approximately 17 times higher than that of pristine Co_3O_4 (Fig. 4e). Fan *et al.*[79] further advanced this strategy by integrating NiO nanosheets with Co_3O_4 nanocages to construct a hierarchical heterostructure with abundant porous channels. This architecture not only preserved the interfacial hole modulation inherent to p–p junctions but also greatly improved gas diffusion and surface reaction kinetics, enabling highly sensitive and rapid detection of NO_2. These studies indicate that although p–p heterojunctions do not exhibit the strong rectifying behavior characteristic of p–n junctions, their gas-sensing performance can still be effectively enhanced through interfacial hole modulation, catalytic promotion, and structural optimization.

3.1.3 Future scope of heterojunction design. Despite their demonstrated effectiveness, heterojunction-based gas sensors face several intrinsic challenges. In practice, the effectiveness of heterojunctions is also strongly influenced by junction density, interfacial continuity, and the dominant conduction pathway within the composite. When charge transport is governed primarily by bulk conduction rather than interfacial barriers, the contribution of heterojunctions to sensing enhancement becomes marginal. This observation further underscores the importance of aligning heterojunction design with nanostructure architecture and transport characteristics.

From a design perspective, effective heterojunction engineering requires precise control over interface chemistry, junction geometry, and phase distribution. Rather than indiscriminate mixing of multiple components, rational designs increasingly emphasize well-defined interfaces, hierarchical architectures, and synergistic integration with catalytic or filtration strategies. When appropriately engineered, heterojunctions serve as powerful transduction amplifiers that convert subtle surface chemical events into robust electrical signals, forming a critical component of next-generation SMO chemiresistive gas sensors.

3.2 Defect and phase control

Defect and phase engineering constitute two closely related strategies for tailoring the sensing behavior of SMO chemiresistive gas sensors by directly modifying their electronic structure and surface reactivity. Unlike heterojunction engineering, which primarily amplifies signal transduction through interfacial barrier modulation, defect and phase regulation act at a more intrinsic level by reshaping the distribution of charge carriers, adsorption energetics, and reaction pathways.

3.2.1 Defect control. Point defects, such as oxygen vacancies, metal vacancies, and heteroatom-induced defect states, are ubiquitous in metal oxides and play a central role in gas-sensing processes.[80] Defects are typically defined as deviations from the ideal periodic arrangement of atoms within a crystal lattice. Although such structural imperfections disrupt the crystallographic order, they simultaneously act as highly active sites for gas–solid interactions.[81] As a result, they play a decisive role in determining the sensitivity and selectivity of gas sensors. Numerous studies have demonstrated that rational defect engineering within SMOs can effectively modulate their electronic structures and carrier-transport behavior, thereby tuning their electrical conductivity.[82]

The introduction of defects greatly increases the density of surficial active sites, providing more favorable conditions for gas adsorption and subsequent surface reactions.[83] Wang *et al.*[84] employed plasma spray technology to prepare SnO_2 nanopowders with finely tunable oxygen vacancy concentrations. By adjusting the spray current, the as-prepared SnO_2 exhibited uniformly distributed nanoparticles, increased specific surface area, and abundant surface oxygen vacancies (Fig. 5a). Notably, the O_{v2}–SnO_2 (preparation current of 600 A) demonstrated a high response of 48 toward 5 ppm NO_2 at operating temperature of 100 °C (Fig. 5b), along with excellent selectivity to NO_2 (Fig. 5c), this technique offers the advantages of a short process flow, high yield, precise vacancy control without external doping, providing a promising new route for the controllable preparation of defect-engineered gas-sensing materials.

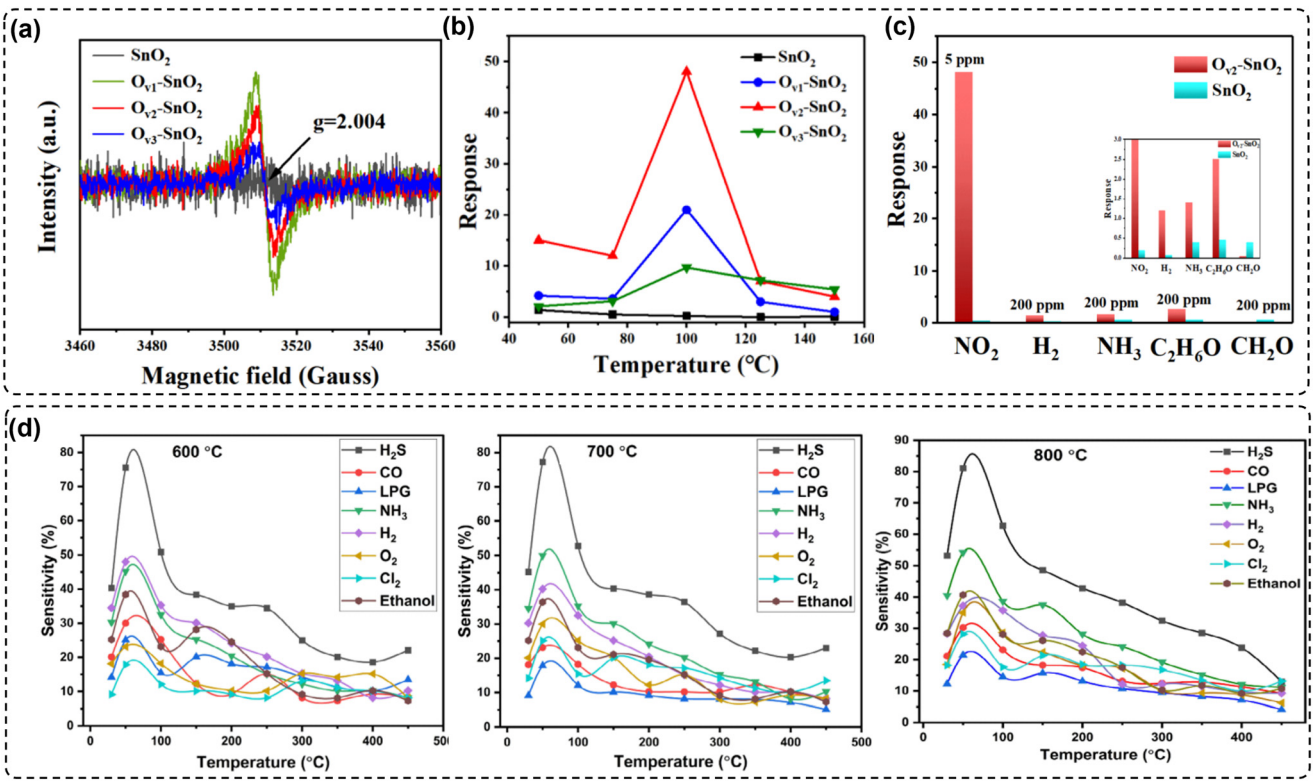

Fig. 5 (a) Electron paramagnetic resonance spectra of each sample. (b) Response of different samples to NO_2. (c) Comparison of responses of O_{v2}–SnO_2 under interference gases. Reproduced with permission.[84] Copyright 2024, American Chemical Society. (d) Sensitivity graph of the La_2O_3 NPs for different gases at different temperatures of 600, 700, and 800 °C. Reproduced with permission.[53] Copyright 2025, Wiley-VCH.

Thermal treatment provides another practical approach to defect modulation. Different annealing temperatures can also lead to varying oxygen vacancies, thereby affecting the gas sensing and sensitivity of the material. Ahemad *et al.*[53] synthesized La_2O_3 using and focused on investigating the effects of different calcination temperatures with 600 °C, 700 °C, and 800 °C. The calcination temperature critically influences the defect states of La_2O_3 nanoparticles: at 600 °C, the particles exhibit oxygen deficiency; at 700 °C, defect concentration remains moderate; while at 800 °C, oxygen vacancies increase substantially, corresponding to the highest level of sensitivity observed. These defects further influence the functionality of material. Oxygen vacancies serve as active sites for gas adsorption, enhancing the sensitivity to H_2S. Specifically, at an operating temperature of 50 °C, the sensitivities of La_2O_3 nanoparticles calcined at 600, 700, and 800 °C exhibited sensitivities of 75.5%, 77.3%, and 81.1%, respectively (Fig. 5d).

Beyond temperature, the calcination atmosphere plays a decisive role in defect formation by controlling the effective oxygen chemical potential.[85] Under high oxygen partial pressure, oxides tend to remain close to stoichiometry, which generally suppresses oxygen-vacancy formation and can favor the formation of cation-related defects such as metal vacancies or higher-valence cation states, depending on the material.[86] In contrast, under reducing conditions, lattice oxygen is more readily removed, and oxygen vacancies often become the dominant defects.[87] In addition to oxygen partial pressure, the chemical reactivity of the atmosphere also matters. If the ambient contains reactive species or impurities, interfacial redox and electron exchange with the oxide may occur, perturbing local charge neutrality and thereby inducing new defect species or stabilizing specific defect configurations. Even nominally inert gases do not react with the oxide, but they can lower the effective oxidizing ability of the environment by diluting oxygen limiting oxygen supply, which in practice can shift defect equilibria relative to calcination in air or oxygen-rich atmospheres.[88]

In parallel, the heating rate regulates defect evolution through kinetic constraints on diffusion, nucleation, and relaxation.[89] With slow heating, the system experiences a longer residence time at intermediate temperatures where defect migration becomes activated. This extended time window enables atoms and point defects to diffuse over longer distances, allowing vacancies and interstitials to recombine, defect clusters to dissolve or coarsen toward lower-energy configurations, and charge compensation to proceed more completely. As a result, the defect population can progressively equilibrate with the local oxygen chemical potential, often yielding a near-thermodynamic defect structure characterized by a relatively low concentration, narrower defect-type distribution, and improved spatial uniformity.[90,91] By contrast, rapid heating compresses the time available for diffusion and equilibration. The lattice is driven quickly across temperature regimes in which defects are generated, but defect annihilation and reorganization cannot keep pace. This kinetic mismatch can trap metastable defect states, promote the retention of quenched-in vacancies, and increase the likelihood of forming complex, non-equilibrium defect ensembles such as defect pairs, clusters, and locally distorted regions.[92,93] Moreover, fast heating can introduce transient thermal gradients and stress, which may further facilitate defect generation or stabilize certain defect configurations. Consequently, a higher overall defect density and a broader spectrum of defect types are often observed, and the resulting defect landscape can be more heterogeneous across grains, surfaces, and interfaces.

Defect stability therefore represents a critical but often overlooked design constraint. Chemical reduction,[94,95] irradiation,[52,96] and thermal treatment[97] can all introduce high defect densities, yet the resulting defect populations may evolve dynamically during sensing cycles. As a result, sensing enhancement achieved through aggressive defect engineering is frequently accompanied by baseline drift and performance degradation. Effective defect design thus requires balancing defect concentration with structural stability, emphasizing controlled generation and stabilization rather than maximal defect density.

3.2.2 Phase control. Phase engineering extends beyond conventional defect control by regulating crystal structure, polymorphism, exposed facets, and phase coexistence within a material.[98] Different crystal phases of the same metal oxide often exhibit distinct electronic structures, surface atomic arrangements, and oxygen-binding characteristics, leading to divergent gas adsorption and reaction behaviors. Single-phase materials with well-defined crystallographic facets allow selective exposure of surface terminations with tailored adsorption energies and reaction pathways. In contrast, multiphase or mixed-phase systems introduce internal phase boundaries that act as additional active regions for charge redistribution and surface reactions. Such phase boundaries can locally modify band alignment, oxygen vacancy formation energy, and carrier transport pathways, thereby enhancing sensing response and, in some cases, selectivity.[99,100]

Hydrothermal method is also commonly used for phase regulation. By controlling the synthesis temperature, Singh *et al.*[101] prepared $MoSe_2$ nanoflowers with tunable 1T/2H phase ratios and constructed CeO_2-based heterostructures. As temperature increased, the metallic 1T phase content decreased from 70% to 14%, while the semiconducting 2H phase became dominant. The crystal phase determines gas selectivity: 1T-rich composites preferentially detect NH_3, whereas 2H-dominated ones are more sensitive to TEA. Under room temperature and 50% RH, the optimal sensor exhibited responses of 45% (1 ppm NH_3) and 58% (1 ppm TEA), with detection limits of 70 ppb and 160 ppb.

Chemical phase composition can also substantially enhance gas-sensing performance. Gangwar *et al.*[102] fabricated mixed-phase p-SnO/n-SnO_2 thin films *via* single-step direct current reactive magnetron sputtering. (X-ray diffraction analysis) XRD, Raman spectra, and (X-ray photoelectron spectroscopy) XPS confirmed the coexistence

of both phases, while Hall measurements demonstrated p-type conductivity at room temperature. Gas-sensing evaluation revealed a temperature-dependent p–n switching behavior toward CO. At low temperatures (50–200 °C), the sensor displayed p-type behavior, with resistance increasing upon CO exposure and a maximum response of 96% at 150 °C. Above the critical temperature of 225 °C, n-type characteristics emerged, featuring resistance decrease and a response of 93% at 325 °C. This unique sensing mechanism stems from the interfacial interactions within the p–n heterojunction: p-SnO governs conduction at low temperatures (hole transport), while n-SnO_2 dominates at higher temperatures (electron conduction). Charge transfer and band bending at the interface synergistically enhance both sensitivity and selectivity toward CO.

However, similar to defect engineering, the benefits of phase regulation are accompanied by intrinsic trade-offs. Metastable phases or phase mixtures may undergo transformation during thermal cycling or long-term operation, leading to changes in electronic structure and sensing behavior. In mixed-phase systems, it is often challenging to decouple the contributions of phase boundaries from those of defects and microstructural heterogeneity, complicating mechanistic interpretation. Consequently, apparent performance enhancement attributed to phase effects may, in practice, arise from coupled defect-phase interactions.[103,104]

3.2.3 Future scope of defect and phase control. Essentially, defect engineering introduces oxygen vacancies, metal vacancies, impurity defects, or lattice distortions to modulate the carrier concentration, tailor surface chemical adsorption, and increase the density of reactive sites. Appropriate oxygen vacancies, not only elevate the electron concentration but also promote the formation of adsorbed oxygen species, thereby accelerating interfacial redox reactions. Phase regulation, on the other hand, alters the phase composition, crystal structure, exposed facets, and crystallographic symmetry, thus reshaping the electronic structure and modifying charge-transport pathways at a more intrinsic level. Both strategies play crucial roles in tuning the sensitivity and selectivity of gas-sensing materials, yet each operates through distinct and complementary mechanisms.

Despite these advantages, defect engineering still faces multiple challenges. Excessive defects often render the lattice thermodynamically metastable, making it susceptible to defect recombination or self-healing during repeated sensing cycles or under humid environments, which leads to signal degradation.[105] Under high temperature working conditions, defects such as oxygen vacancies may diffuse, migrate, or even trigger local phase reconstruction, causing defect densities to fluctuate uncontrollably. In addition, heteroatom dopants can introduce additional charge carriers and enhance chemisorption; however, the stability of dopant states, their spatial distribution, and the risk of secondary-phase formation remain difficult to control. Overall, although defect engineering has driven substantial progress in sensing enhancement, issues such as poor selectivity, limited long-term stability, and uncontrolled defect evolution persist.

Phase regulation faces similar challenges in terms of synthesis precision and structural stability. Because different crystal phases display substantial variations in electronic structure, surface polarity, and vacancy formation energy, minor fluctuations in synthesis conditions, such as temperature, duration, or precursor ratio can lead to significant differences in phase fraction, grain size, and interfacial characteristics. In multiphase composite systems, performance improvements are often attributed to interfacial charge redistribution, modified oxygen adsorption energetics, or enhanced interfacial catalysis. However, the underlying reaction mechanisms and the quantitative contributions of these effects remain unclear, and the dynamic processes occurring at phase boundaries are still insufficiently understood.

From a design perspective, the key challenge lies in identifying optimal defect and phase configurations that balance reactivity with structural robustness. This requires precise control over synthesis conditions, defect distribution, and phase fraction, as well as careful evaluation under realistic operating environments. Rather than pursuing extreme defect densities or highly metastable phases, future efforts are expected to focus on stabilized defect states, controlled phase coexistence, and synergistic integration with heterojunction, catalytic, or filtration strategies to achieve sustainable sensing performance.

3.3 Noble metal catalysts

Noble metal catalysts have been extensively employed to enhance the gas sensing performance of SMO chemiresistive sensors, primarily by accelerating surface reactions and modulating interfacial charge transfer. From a mechanistic standpoint, noble metals do not introduce new sensing principles; rather, they reshape the kinetics and energetics of existing oxygen-mediated redox pathways and strengthen the coupling between surface chemistry and electrical transduction.

3.3.1 Noble single atom catalysts. Single-atom catalysts (SAC) refer to a catalytic configuration in which noble metal atoms are anchored on metal-oxide supports in an atomically dispersed state, ideally without forming clusters or nanoparticles. This ultrahigh dispersion maximizes atomic utilization efficiency, ensuring that each individual atom functions as an isolated reactive site while simultaneously contributing to an increased specific surface area.[55] Owing to their unsaturated coordination environment and discrete electronic states, these single atom sites exhibit exceptionally strong adsorption capability and highly effective activation toward gas molecules.[106,107] As shown in Fig. 6a, Feng *et al.*[108] dispersed gold nanoparticles onto mesoporous SnO_2 nanospheres to construct a composite structure featuring Au–O–Sn active sites. The resulting material exhibits a uniform spherical morphology, large pore size, and a high

specific surface area. The fabricated SnO_2/Au-SAs-0.6% (SnO_2 loaded with 0.6% Au atoms) sensor demonstrates an outstanding response of 587.3% toward 2 ppm 3-hydroxy-2-butanone (3H-2B) at a low operating temperature of 50 °C, which is 183.5 times higher than that of pristine mesoporous SnO_2 (Fig. 6b). It also achieves an ultralow detection limit of 10 ppb, a rapid response time of only 10 s, and excellent selectivity, repeatability, and long-term stability. Density functional theory (DFT) calculations further reveal that Au single atoms markedly enhance the adsorption strength and charge-transfer efficiency between SnO_2 and 3H-2B, thereby boosting the sensing performance (Fig. 6c).

Moreover, charge transfer between single atoms and the oxide support perturbs the local electronic structure, introducing impurity states or modifying band bending near the surface. Even at extremely low loadings, the presence of single atoms can markedly regulate surface band bending and the width of the depletion layer, directly influencing the baseline resistance of the metal oxide semiconductor.[109] For instance, Qian *et al.*[110] stabilized Pd single atoms on the surface of hollow porous SnO_2 nanospheres through electrostatic adsorption followed by high-temperature calcination, forming a well-defined Pd–O–Sn coordination structure. The incorporation of Pd single atoms introduces a new impurity energy level near the conduction band minimum of SnO_2, significantly reducing the electron transition barrier and thereby greatly increasing the concentration of free charge carriers in the material (Fig. 6d). Meanwhile, hybridization occurs between the 4d orbitals of Pd and the 2p orbitals of adjacent oxygen atoms near the Fermi level (Fig. 6e), which stabilizes the isolated Pd atoms but also markedly promotes the activation and dissociation of the O═O bond in adsorbed oxygen molecules.

Furthermore, SACs often provide unique catalytic pathways. The tailored orbital hybridization between the single atom and the support enables the formation of new reaction intermediates and reduces the activation energy for rate-determining steps, such as oxygen adsorption, dissociation, and the interconversion between $O_2^-/O^-/O^{2-}$ species. This atomically precise catalytic promotion accelerates the generation of active oxygen species, enhances the efficiency of charge exchange between adsorbates and the sensing layer, and enables the selective activation of specific gas molecules.[111] For example, Pt single atoms uniformly deposited on the surface of SnO_2 can induce a pronounced oxygen spillover effect, which facilitates the dissociation of O_2 into highly reactive O^- species. Through this oxygen spillover effect, Pt significantly enhances the kinetics of

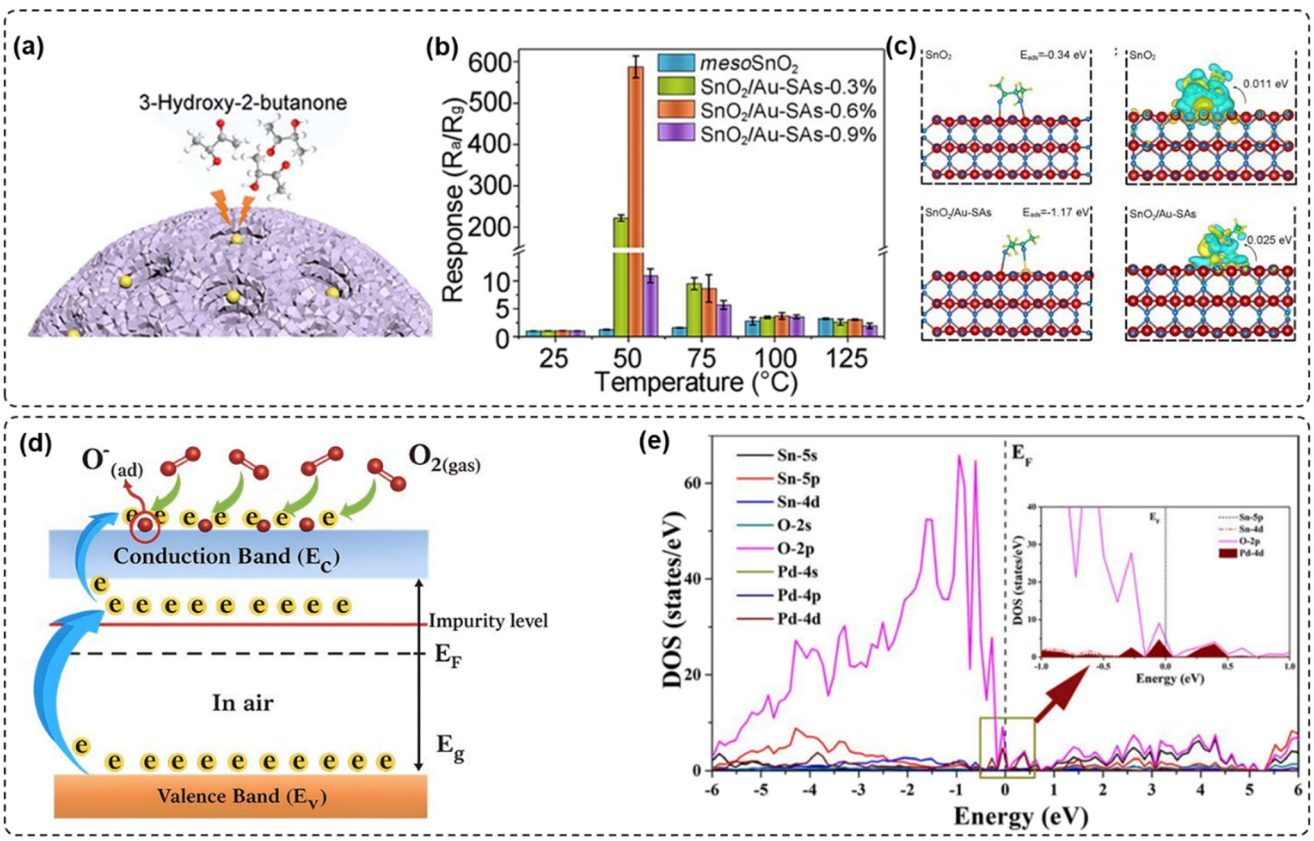

Fig. 6 (a) Single-atom Au-functionalized mesoporous SnO_2 nanospheres. (b) Response toward 2 ppm of each sample at different temperatures. (c) Adsorption energy and its charge density difference of 3H-2B for SnO_2, SnO_2/Au-SAs. Reproduced with permission.[108] Copyright 2024, American Chemical Society. (d) Mechanism of SnO_2/Pd_{atom} in air. (e) The partial density of states for SnO_2/Pd_{atom}. Reproduced with permission.[110] Copyright 2025, Qian *et al.*

surface redox reactions, thereby enabling ultrasensitive gas detection with rapid response characteristics.[112]

By lowering the energy barriers for gas–solid reactions, SACs facilitate rapid response and recovery kinetics, high sensitivity, and superior selectivity even under mild or near-ambient conditions. However, single atoms are typically in a high surface energy, unsaturated coordination state. Under high temperature operating conditions and in strongly reducing or oxidizing atmospheres, they are prone to surface diffusion and further agglomeration into nanoclusters or nanoparticles. This leads to a decrease in the number of active sites, changes in electronic structure, thus weakening its unique advantages in gas sensing.[113,114] Moreover, due to the high requirements for cost, response stability, and long-term cycling performance in gas sensing, single atoms are usually introduced into the system at extremely low loading levels. With insufficient loading or uneven distribution, the electronic structure modulation and surface reaction promotion effects induced by single atoms are often limited, making it difficult to demonstrate a significant advantage in macroscopic resistance signals.[115] The sensing response remains primarily dominated by the intrinsic properties of the carrier. Therefore, how to achieve controllable loading increases and synergistic amplification effects while ensuring high dispersion and structural stability of single atoms has become one of the core scientific problems facing single-atom catalytic gas sensors.

By intentionally introducing electron-deficient defects into metal oxide supports, these defects can serve as atomic-level anchoring sites with high binding energy, forming stable coordination structures with metal atoms.[116] This can significantly suppress the migration and aggregation of single atoms under high-temperature or complex atmospheric conditions. Simultaneously, by controlling the specific surface area and surface active sites density of the support, more available sites can be provided for single atom anchoring, achieving higher and controllable loading while ensuring atomic-level dispersion.[117] This amplifies the regulatory effect of single atoms on the overall electronic structure and surface reaction kinetics. Furthermore, employing deposition strategies with precisely controllable growth kinetics, such as electrochemical deposition,[118] photochemical reduction,[119] atomic layer deposition,[120] or plasma-assisted deposition,[121] it is expected to achieve uniform, localized, and repeatable loading of single atoms on the surface of pre-constructed sensor devices or sensitive layers. The synergistic implementation of these strategies provides a feasible path to leverage the advantages of SAC in gas sensing at the practical device level.

3.3.2 Noble metal nanoparticles catalysts. Noble metal nanoparticles (NPs) typically exist on metal oxide surfaces in the form of multi-atom aggregates and are mainly composed of noble metals such as gold, silver, and platinum. Owing to their high specific surface area, these nanoparticles exhibit outstanding catalytic activity. As the particle size decreases, the proportion of surface atoms increases markedly, leading to the exposure of a greater number of active sites.[122,123] The catalytic activity of NPs arises from the abundance of low-coordination atoms at edges and corners, which facilitate gas adsorption, bond activation, and reaction turnover.[124,125]

As active centers, the core mechanism of noble metal NPs lies in their ability to lower the activation energy for the adsorption, dissociation, and transformation reactions of gas molecules on the metal oxide surface. On a microscopic level, the heterojunction between the noble metal NP and the metal oxide induces electron transfer, alters the electronic state density of the metal oxide surface, and optimizes the adsorption configuration of gas molecules. When gas molecules contact the surface, noble metal NPs modulate the chemical bond strength of the gas molecules through electron transfer, lowering the reaction energy barrier, enabling the reaction to proceed at a lower temperature, significantly improving the reaction kinetics, suppressing side reactions, and enhancing catalytic selectivity and stability.[126]

At the metal oxide interface, NPs form Schottky barriers that modulate electron transport across the junction. The height and width of these barriers are sensitive to surface charge variations induced by gas adsorption and reaction, amplifying resistance changes upon exposure to target analytes. In addition, noble metal NPs can induce spillover effects, whereby activated oxygen species migrate from the metal surface to the oxide support, extending the reactive region beyond the immediate metal–gas interface.[127] For example, Yan *et al.*[128] modified tin oxide nanotubes with different metals to form Schottky barriers and enhanced gas response through electronic and chemical sensitization (Fig. 7a), combined with the support vector machine algorithms, successfully achieving 100% accurate classification of H_2, formaldehyde, toluene and NO_2 (Fig. 7b).

The nanoscale size of noble metal particles endows them with several unique surface advantages that significantly enhance their catalytic and gas-sensing properties. As the particle size decreases, the ratio of edge and corner atoms relative to the total number of atoms increases. These edge atoms, which are typically less coordinated and have higher energy states, play a crucial role in improving the reactivity of the particles. This leads to an uneven distribution of the electron cloud, which further enhances their chemical activity. The increased concentration of active sites at the particle surface allows for stronger interactions with reactant molecules, promoting faster adsorption, dissociation, and transformation processes. By controlling the morphology and size of NPs, it becomes possible to fine-tune the distribution and density of these active sites.[129] For instance, by synthesizing nanoparticles in specific shapes such as spheres, rods, or cubes, it is possible to optimize the number of surface atoms that are available for catalysis.[130] This structural control allows for better management of the electron density at the particle surface, which in turn influences electronic structure of material. Through such control, the efficiency of gas molecule adsorption and transformation can be enhanced, leading to higher catalytic

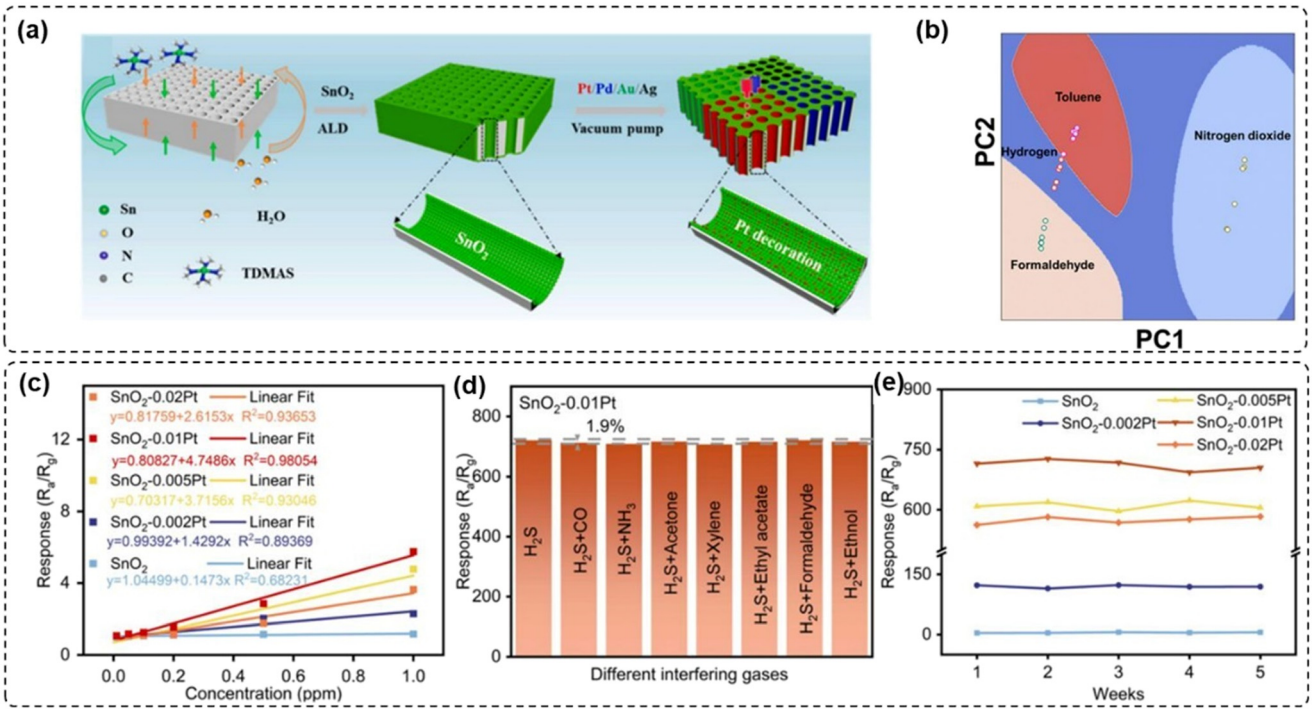

Fig. 7 (a) The schematic process for 3D SnO_2 nanotube fabrication and metal decoration. (b) Gas classification of H_2, formaldehyde, toluene and NO_2 employing support vector machine. Reproduced with permission.[128] Copyright 2024, Elsevier. (c) Response curves of all samples to different concentrations of H_2S at 25 °C. (d) Response values of SnO_2 and SnO_2-0.01 Pt to the mixture of 10 ppm of H_2S and 10 ppm of interfering gas at 25 °C. (e) 5 weeks stability test of all samples to 10 ppm of H_2S at 25 °C. Reproduced with permission.[131] Copyright 2024, American Chemical Society.

activity and improved gas-sensing performance. Furthermore, adjusting the particle size and morphology can influence the interaction between the noble metal and the support material, leading to better charge transfer, enhanced stability, and increased sensor selectivity.

The amount of metal loading has a significant impact on sensing performance, and its effect is not a simple linear enhancement relationship. Zou *et al.*[131] decorated a MOF-derived porous SnO_2 matrix with Pt nanoparticles to elucidate the critical role of Pt loading in regulating sensor behavior. By precisely tuning the Pt content, it was demonstrated that the sensing performance does not increase monotonically with increasing metal loading; instead, an optimal loading threshold exists (Fig. 7c). When the Pt loading exceeds this optimum, Pt nanoparticles tend to aggregate, resulting in a deterioration of sensing performance. At the optimal loading level (SnO_2-0.01 Pt), the sensor exhibits excellent overall performance, delivering an ultrahigh response of 721% toward 10 ppm H_2S (Fig. 7d), together with good long-term stability and durability (Fig. 7e).

The sensing performance of NP-decorated systems exhibits a strong dependence on particle size, dispersion, and loading amount. Excessive metal loading can lead to particle aggregation, reduced effective surface area, and even the formation of metallic conduction pathways that short-circuit resistance modulation. Consequently, an optimal loading window typically exists, within which catalytic promotion and electronic sensitization are maximized without compromising transduction efficiency.

3.3.3 Future scope of noble metal catalysts. Noble-metal catalysts have been widely introduced into gas-sensing systems and has shown clear advantages in accelerating reaction kinetics and improving sensitivity. However, several practical bottlenecks remain for device development and large-scale implementation. Noble metals are susceptible to catalytic poisoning and deactivation. When exposed to sulfur-containing species such as H_2S and SO_2, noble-metal surfaces can undergo strong and largely irreversible chemisorption or sulfide-forming reactions, which block or destroy active sites, leading to baseline drift, response attenuation, and even permanent performance degradation.[132] To address this issue, a practical strategy is to construct a protective layer or a selective interfacial barrier, to encapsulate noble-metal nanoparticles with an ultrathin yet porous coating. Such a coating provides diffusion channels and defect pathways that allow small target-gas molecules and O_2 to rapidly access the active interface, while partially suppressing the direct contact between sulfur species and the noble metal, thereby reducing the likelihood of irreversible poisoning and improving long-term stability. In addition, the protective layer can be coupled with strong-anchoring strategies by enhancing the metal–support interaction to inhibit migration and aggregation during operation, mitigating the loss of effective surface area and active-site density.

Moreover, noble-metal nanoparticles/clusters tend to migrate and aggregate during thermal treatment or long-term operation, reducing the effective surface area, diminishing the density of active centers, and weakening interfacial catalytic effects, so the initial performance gains are difficult to sustain.[133] To address this issue, on one hand, the interaction between noble metals and metal oxide supports can be enhanced by constructing defect anchoring sites. For example, introducing an appropriate amount of defects such as oxygen vacancies, metal vacancies, or distorted lattices on the support surface can provide a stronger chemisorption/coordination environment, enabling noble metals to preferentially nucleate at these high energy sites and become stably immobilized. Simultaneously, the strength of metal–support interactions can also be improved through heteroatom doping or interfacial bonding. This significantly reduces the surface diffusion and migration tendency of noble metals under thermal treatment and long-term working conditions, thereby achieving a more durable highly dispersed state and stable interfacial catalytic effects. On the other hand, spatial confinement and structural isolation strategies can be employed to limit the "freedom of movement" of noble metals, inhibiting particle growth and aggregation without compromising gas mass transfer.

The design philosophy for noble metal catalysis is expected to evolve from single metal toward multi-metal cooperative architectures. On one hand, conventional single-metal catalysts can be extended to catalytic configurations supported by two or more metal atoms, including dual-atom sites, heteronuclear bimetallic pairs, and sub-nanometer alloy clusters.[134] For example, one metal can preferentially promote O_2 dissociation and the generation of reactive oxygen species, whereas another metal can enhance the adsorption and bond cleavage of target gases, thereby enabling tandem catalytic pathways. On another hand, multi-metal sites provide diverse coordination environments, allowing sensing materials to exhibit distinguishable kinetic signatures toward different analytes and promoting multi-gas detection and identification. Importantly, multi-metal systems can improve the balance among sensitivity, selectivity, and poisoning resistance through interfacial electronic-structure regulation and intermediate-binding optimization, mitigating the common trade-off observed in single-metal catalysts.[135,136]

In parallel, integrating noble metal catalysis with heterojunction architectures represents another promising direction. Noble metals, including nanoparticles, sub-nanometer clusters, and single atoms, can form Schottky-type contacts or strong interfacial charge-transfer regions with metal oxides, while oxide–oxide heterojunctions introduce additional band bending and space-charge-layer modulation. Their integration can yield synergistic catalytic and electronic sensitization. Noble metals reduce reaction barriers and accelerate surface redox kinetics, whereas heterojunctions amplify resistance modulation by strengthening interfacial barrier variations and improving carrier separation and transport. Furthermore, heterointerfaces can act as reaction-active regions that facilitate efficient coupling among gas adsorption, surface reaction, and electrical transduction. With rational spatial design, such as preferentially anchoring noble metals at heterojunction interfaces or constructing multi-junction and triple-phase interfaces, high low-temperature response can be maintained while further enhancing selectivity and long-term stability, offering an engineering-feasible pathway toward low-power, interference-resistant, and durable gas sensors.

3.4 Gas filtration

Gas filtration provides a fundamentally different strategy for improving selectivity in SMO chemiresistive gas sensors by decoupling gas discrimination from the intrinsic response of the sensing layer. Unlike material-centered approaches that modify surface chemistry or charge transport within the SMO itself, filtration strategies regulate which gas species reach the sensing interface and in what chemical form. From a mechanistic perspective, gas filtration effectively reprograms the sensing pathway by controlling molecular flux, reaction sequence, and competitive adsorption prior to charge transduction.

3.4.1 Sorption and molecular-sieve gas filtration. Sorption and molecular-sieve gas filtration is a widely used strategy for improving the selectivity of gas sensors. The central concept is to introduce a filtering medium in front of the sensing layer so that an adsorbent selectively captures and retains interfering species through physisorption and weak chemical interactions.[137] By suppressing cross-responses, the target analyte reaches the active sensing material with a higher effective partial pressure and reduced competition for adsorption sites, thereby enhancing selectivity and improving signal reliability.[138] In general, sorption and molecular-sieve gas filtration is not intended to alter the intrinsic chemical identity of the gas molecules or to change their reaction pathways. Instead, separation is primarily achieved through intermolecular interactions and transport-based sieving effects.[139] Although both are typically regarded as physical, transport-dominated approaches, they differ fundamentally in selectivity mechanisms, capacity and kinetic limitations, failure modes, and key design parameters.

For adsorption-based filtration, the operating principle relies on selective adsorption driven by intermolecular interactions. Separation is achieved by exploiting differences in dipole–dipole interactions, polarizability, acid base affinity, and reversible coordination between the adsorbent and various gas molecules. As a result, interfering species can be preferentially enriched and retained, thereby mitigating competitive adsorption and false triggering at the sensing layer.[140] Common adsorbents include carbon-based,[141,142] metal–organic frameworks (MOFs),[143] and covalent organic frameworks (COFs).[144] These materials typically feature high specific surface areas, abundant micro/meso-porous networks, and tunable pore-size

distributions and surface chemistries. Through functional-group engineering, or the introduction of specific metal sites, they can exhibit higher adsorption affinity and faster adsorption kinetics toward selected molecules, creating an effective selectivity window for filtration. For instance, Hwang *et al.*[145] used microporous poly(dimethylsiloxane) (PDMS) as a porous scaffold and incorporated two functional MOFs of Cu(BTC) and MIL-160. This approach yielded a gas-filtering system featuring a high specific surface area and three-dimensionally interconnected open pores (Fig. 8a). Under mixed atmospheres containing H_2, CO, and humidity of 40%, integrating the two filters effectively suppressed cross-interference from CO and moisture, leading to a maximum 7.9-fold enhancement in H_2 selectivity (Fig. 8b). This result highlights the effectiveness of multifunctional filtration layers for selectivity amplification in multicomponent environments.

Meanwhile, molecular sieve filtration serves as an efficient front-end preprocessing strategy for gas sensing.[146] Its selective permeation is primarily determined by both the structural parameters of the filtering layer and the characteristics of gas molecules, with key factors including membrane thickness, pore size and distribution, pore connectivity and tortuosity, as well as the kinetic diameter of gas molecules.[147] Specifically, when the kinetic diameter of the target gas matches the pore size of the molecular sieve more closely and it exhibits a higher diffusion coefficient within the pores, the target molecules can preferentially pass through the molecular sieve layer with lower diffusion resistance and reach the sensing active layer.[148] In contrast, interfering gases with larger kinetic diameters or stronger interactions with the pore walls, which lead to restricted diffusion, are subject to size exclusion, adsorption retention, or significant delay, thereby reducing cross-sensitivity and

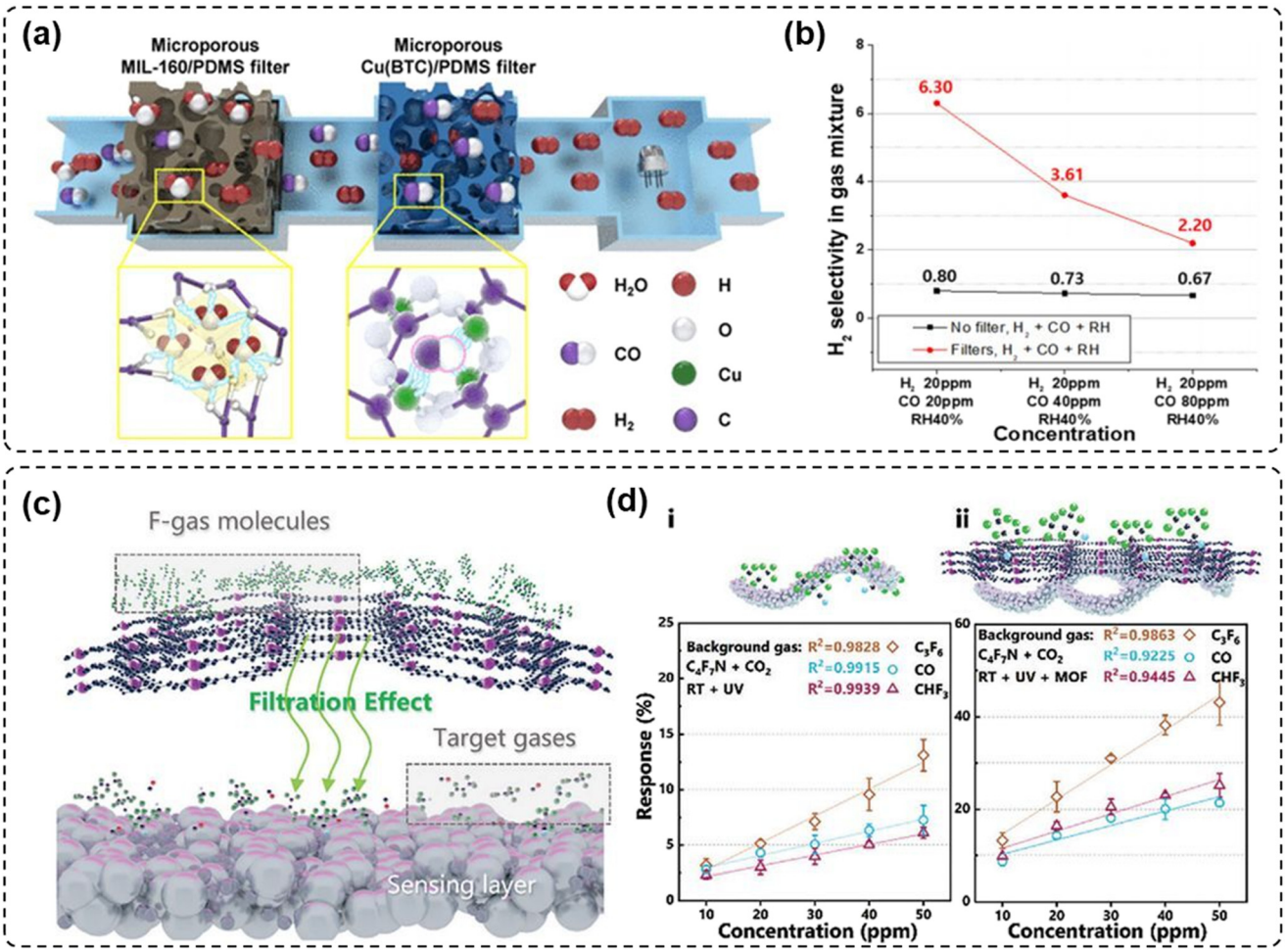

Fig. 8 (a) Schematic image of a filtering system based on a microporous elastomer filter coated with MOFs. (b) Selectivity to the mixture of 20 ppm H_2 gas, RH 40% air, and 20/40/80 ppm CO gas with/without microporous Cu(BTC)/PDMS and MIL-160/PDMS filters. Reproduced with permission.[145] Copyright 2020, American Chemical Society. (c) Bilayer design for effective detection of impurities gases in F-gas environment. (d-i) Gas-sensing characteristics of SnO_2 NFs sensor at RT under 94%CO_2/6%C_4F_7N atmosphere and UV irradiation. (d-ii) Gas-sensing characteristics of $Co_3(HITP)_2/SnO_2$ sensor at RT under 94%CO_2/6%C_4F_7N atmosphere and UV irradiation. Reproduced with permission.[57] Copyright 2025, Wiley-VCH.

improving selectivity.[149] Table 3 summarized some gas kinetic diameters and chemical properties.

Compared to adsorption-based filtration, the selectivity of molecular sieve filtration relies more on the mass transfer sieving effect resulting from pore size exclusion and diffusion differences, thus often exhibiting a clearer sieving threshold and faster dynamic response. However, this approach also requires a trade-off between selectivity and flux, as excessively thick or dense membrane layers may lead to slower response times and increased pressure drop. Additionally, molecular sieve layers are sensitive to humidity, water molecules may compete to occupy the pores or cause pore blockage, leading to drift in sieving performance.[150] Therefore, in practical applications, pore or surface chemistry modulation or hydrophobic modification is often employed to enhance their stability and reproducibility in complex environments.

Coupling microporous diffusion-based sieving with selective adsorption is an effective strategy to enhance the selectivity of gas sensors under strong background interference. Recently, Wu *et al.*[57] proposed a UV-activated, bilayer filtration-sensing architecture, where a 2D MOF, $Co_3(HITP)_2$, serves as an overlayer-type selective filtering film on top of SnO_2 nanofibers, enabling room-temperature detection of trace impurities (C_3F_6, CO, and CHF_3) in a C_4F_7N/CO_2-dominated background (Fig. 8c). This overlayer provides high-flux microporous pathways that allow impurity molecules to permeate, while preferentially adsorbing and immobilizing the background C_4F_7N *via* strong interactions between Co sites and the –CN group (Fig. 8d), thereby substantially suppressing C_4F_7N interference and improving the detectability and detection-limit performance of the target trace gases under harsh background conditions.

3.4.2 Catalytic gas filtration. Sorption and molecular-sieve gas filtration methods generally rely on the premise that the target analyte and interfering species exhibit amplifiable differences in kinetic diameter, molecular shape, or polarity/solubility/adsorption affinity. However, under many practical conditions, the gases to be discriminated often feature similar kinetic diameters and comparable chemical properties, making it difficult for purely non-reactive filtering to generate a sufficiently large flux contrast; consequently, selectivity enhancement becomes severely constrained. To address this limitation, catalytic filtering has been developed, in which a catalytically functional layer is placed either at the inlet of the sensor chamber or directly on the sensing element. In this configuration, the gas mixture undergoes a controllable catalytic reaction before reaching the sensing layer, thereby actively reshaping the composition and reactivity of the incoming gases and amplifying selectivity.[161,162] Practically, the catalytic filter can be regarded as a chemical pretreatment layer: rather than physically blocking gas transport, it exploits differences in activation barriers, adsorption/desorption kinetics, and reaction pathways on the catalyst surface to achieve reaction-selective routing of mixed gases.

Table 3 Dynamic diameters of common gases

Gases	Dynamic diameters (nm)	Ref.
H_2	0.283	151
CH_4	0.380	152
N_2	0.364	153
He	0.260	154
C_3H_6	0.430	154
NO_2	0.330	155
SO_2	0.410	155
H_2S	0.360	156
Ethanol	0.446	157
H_2O	0.260	158
Acetone	0.460	159
NH_3	0.330	138
CO_2	0.330	160

One common implementation introduces catalytic components that preferentially oxidize or convert more reactive interferents into products that induce much weaker sensor responses, thereby suppressing nonspecific responses originating from interfering gases.[164] In contrast, the target analyte exhibits a relatively low conversion within a properly selected temperature/residence-time window, allowing it to pass through the filter and be detected by the downstream sensing material. Catalytic filtering is often more effective than purely physical separation when discriminating gases with similar sizes and similar chemical characteristics, and it is better suited for interference mitigation under complex real-world conditions. For example, Jeong *et al.*[56] employed Rh–SnO_2 hollow spheres as the sensing layer and deposited an approximately 0.4 μm thick CeO_2 catalytic overlayer to form a bilayer structure (Fig. 9a and b). The CeO_2 layer catalytically oxidizes highly reactive non-aromatic interferents into low-activity or inactive products at relatively low temperatures, whereas structurally stable aromatic hydrocarbons can permeate through the overlayer and react on the underlying Rh–SnO_2 film. As a result, the device exhibits a high response to 5 ppm aromatic hydrocarbons at 300 °C while showing negligible responses to interferents, demonstrating excellent selectivity (Fig. 9c).

Another catalytic-filtering mode works on the catalytic layer selectively activates or partially converts the target analyte without fully consuming it into an intermediate that is more readily detected by the downstream sensing material.[165] In this case, the catalytic layer reduces the effective energy barrier of subsequent reactions or alters adsorption configurations and reaction pathways, enabling more efficient charge transfer and surface redox processes on the sensing layer, thereby increasing response magnitude and potentially accelerating response dynamics. As shown in Fig. 9d, Xue *et al.*[163] designed a core–shell, cascade catalytic-enhancement gas sensor based on the concept of "primary catalytic reforming, secondary oxidation sensing". Specifically, a $Ce(OH)_x$ shell with a tunable mesoporous architecture was precisely conformally coated onto the surface of hollow cubic $CoSn(OH)_6$ cores *via* a confined interfacial co-assembly method to form a precursor (Fig. 9e). Subsequent annealing under a nitrogen atmosphere

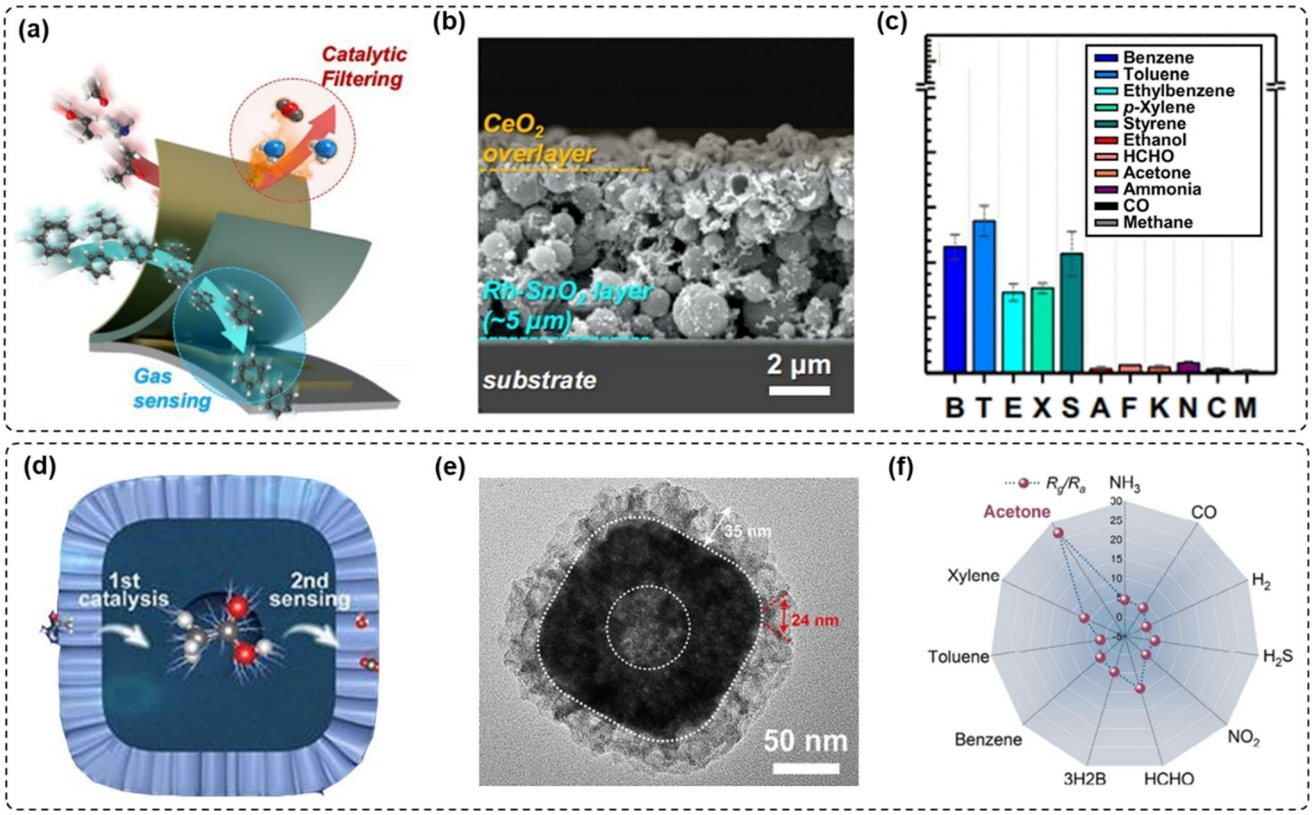

Fig. 9 (a) Bilayer sensor with catalytic CeO_2 overlayer. (b) Cross-sectional SEM images of CeO_2/Rh–SnO_2 film. (c) Gas-sensing characteristics of 0.4CeO_2/Rh–SnO_2 in different gases at 5 ppm. Reproduced with permission.[56] Copyright 2023, Jeong *et al.* (d) Schematic illustration of tandem catalytic reforming-oxidation sensing mechanism. (e) TEM images of $CoSn(OH)_6$@m$Ce(OH)_x$. (f) Selectivity investigation of $CoSnO_3$@mCeO_2-2 sensor toward 50 ppm various gases at 260 °C. Reproduced with permission.[163] Copyright 2025, Wiley-VCH.

converted the precursor into a single-particle cascade catalytic-sensing platform. Mechanistically, as acetone traverses the oxygen-vacancy-rich mCeO_2 catalytic shell, it is preferentially and selectively reformed into a more reactive acetic-acid intermediate. The acetic acid then diffuses into the interior $CoSnO_3$ sensing core, where it undergoes vigorous oxidation, thereby markedly amplifying the chemiresistive signal. Owing to this distinctive spatially partitioned design and cascade reaction pathway, the sensor delivers ultrahigh sensitivity and excellent selectivity toward acetone, while exhibiting negligible cross-responses to a variety of interfering volatile organic compounds (Fig. 9f).

Notably, the key bottleneck of this strategy lies in achieving precise matching. If the catalytic layer is overly active or if the residence time of the target gas within the filter layer is too long, the target molecules may be excessively converted or even completely mineralized, leading to a decrease in the effective analyte flux reaching the sensing layer. This ultimately manifests as attenuation of the response amplitude or even reduced sensitivity. Conversely, if the catalytic activity is insufficient, it becomes difficult to generate a stable and reproducible flux of intermediates under the set operating conditions, thereby failing to achieve the intended signal amplification. Furthermore, the catalytic window is jointly constrained by factors such as temperature, oxygen partial pressure, humidity, and flow rate, meaning that the desired state of often exists only within a relatively narrow operating range. Achieving optimal performance requires the coordinated optimization of catalyst composition, support pore structure, coating thickness, and flux/residence time.

3.4.3 Future scope of gas filtration. Gas filtering is an effective way to mitigate interference in mixed and contaminated atmospheres because it conditions the gas stream before it reaches the sensing layer. However, a single filtering mechanism is rarely sufficient to meet the increasingly diverse requirements of future gas detection across multiple targets, environments, and interference backgrounds. Therefore, multistage and multilayer processing strategies are expected to become more important. By assigning clear functions to different layers, for example removing humidity and background species first and then performing molecular sieving followed by catalytic conversion or preconcentration, or by designing composite filtering media that couple multiple selectivity mechanisms within one layer, such architectures can substantially improve selectivity and robustness in complex gas mixtures.

Humidity poses a particular challenge for filtration-based designs. Many porous and sorptive materials exhibit strong affinity toward water vapor, which can occupy pores,

deactivate adsorption sites, and severely reduce gas permeability. Consequently, filtration layers must be carefully designed to maintain gas flux and selectivity under humid conditions. Strategies such as hydrophobic surface modification, hierarchical pore construction, and humidity-tolerant catalytic filters have been explored to mitigate water-induced deactivation. These considerations highlight that filtration performance is intrinsically coupled to humidity management rather than being an independent function.

The thickness, porosity, and placement of filtration layers further influence sensor performance. Excessively thick or dense filters can impede gas diffusion, leading to prolonged response and recovery times, while overly thin layers may provide insufficient selectivity enhancement. In integrated sensor architectures, filtration layers are increasingly positioned as overlayer-type components or spatially separated modules, enabling independent optimization of filtration and sensing functions. Such modular designs offer greater flexibility in balancing selectivity, sensitivity, and response dynamics.

Despite their advantages, filtration strategies introduce additional complexity in device fabrication and long-term stability. Adsorption-based filters may saturate over time, while catalytic filters can suffer from deactivation or structural evolution. Regeneration capability, durability, and compatibility with low-power operation therefore represent critical design constraints. From a broader perspective, gas filtration should be viewed not as a standalone solution but as a complementary strategy that synergistically enhances the effectiveness of heterojunction engineering, defect regulation, and catalytic sensitization. When judiciously integrated, filtration layers enable chemiresistive sensors to operate beyond the intrinsic selectivity limits imposed by oxygen-mediated sensing mechanisms.

3.5 Nanostructure

3.5.1 Nanostructure design. Nanostructure design has been widely adopted in the design of metal-oxide sensing materials.[166] The essence lies in tailoring the physicochemical processes involved in gas sensing by nanostructuring materials across different dimensionalities and architectures. Rather than serving solely to increase surface area, nanostructuring fundamentally regulates mass transport, surface reaction accessibility, and charge-transport pathways, thereby shaping both the magnitude and dynamics of the sensing response.[167] Metal-oxide nanostructures are commonly categorized into 0D, 1D, 2D, and 3D morphologies, each associated with distinct mass-transport behaviors, interfacial characteristics, and charge-transport pathways.[168] Notably, morphological tuning serves as a structural carrier that synergizes with doping, defect engineering, heterojunction construction, and surface functionalization.

0D structures generally refer to nanoparticles with characteristic dimensions typically below 100 nm in all three directions.[169] Their high specific surface area provides abundant active sites for gas–solid reactions. When the particle size becomes comparable to the Debye length, modulation of the space-charge region can extend throughout the entire particle, thereby amplifying the resistance change induced by gas adsorption.[170] In practice, 0D components usually play three roles: (i) serving as the primary building blocks of porous sensing films for direct gas detection; (ii) acting as functional additives in other sensing matrices to regulate electron distribution or introduce defects, thus improving sensitivity and selectivity; and (iii) functioning as supports synergistic sections for noble-metal nanoparticles, providing additional enhancement *via* electronic sensitization and catalytic effects.[171–174]

1D structures benefit from a high aspect ratio and directional charge-transport channels.[175] They offer continuous axial pathways for efficient carrier transport while providing a large external surface area for gas adsorption, often leading to faster response/recovery dynamics and improved charge-transport properties compared with 0D nanoparticles.[176] Moreover, 1D architectures are particularly amenable to surface modification and heterojunction construction, enabling further tuning of surface chemical activity and band-structure rearrangement to substantially enhance sensitivity and selectivity.[177] For example, Shin *et al.*[54] used one-dimensional SnO_2 nanostructures as carriers, in which platinum single atoms were first anchored on carbonitride nanosheets, and the resulting composite was then embedded into electrospun SnO_2 fibers (Fig. 10a). Subsequent calcination yielded a fibrous tubular structure rich in heterojunction interfaces. This approach achieved high dispersion and uniform distribution of platinum, while the confinement effect from the heterojunction interfaces prevented the aggregation of platinum single atoms. The resulting Pt-MCN-SnO_2 material exhibited outstanding performance in formaldehyde gas sensing, surpassing conventional Pt-doped or pure SnO_2 systems (Fig. 10b).

2D metal-oxide systems exhibit pronounced planar advantages owing to their atomic-level thickness and lateral extension. In chemiresistive sensors, they can simultaneously act as interfacial modulation layer, efficient electron-transport channel, and designable adsorption interface. Their high surface area facilitates gas access to active sites, while surface defects, functional groups, and edge sites can provide selective adsorption and reaction centers for specific analytes. Meanwhile, heterointerfaces formed between 2D sheets (*e.g.*, MXene, graphene/graphene oxide, and MoS_2) and metal oxides can induce charge transfer and band bending, effectively modulating depletion layers and barrier heights and thereby amplifying resistance changes upon gas adsorption. In addition, continuous 2D conductive networks can reduce operating temperature, accelerate response/recovery, and improve cycling stability.[178–181] Nevertheless, excessive restacking or dense encapsulation should be avoided, as it may block diffusion pathways and deteriorate mass-transport efficiency.

3D structures are frequently employed as porous microspheres, hollow architectures, or core–shell

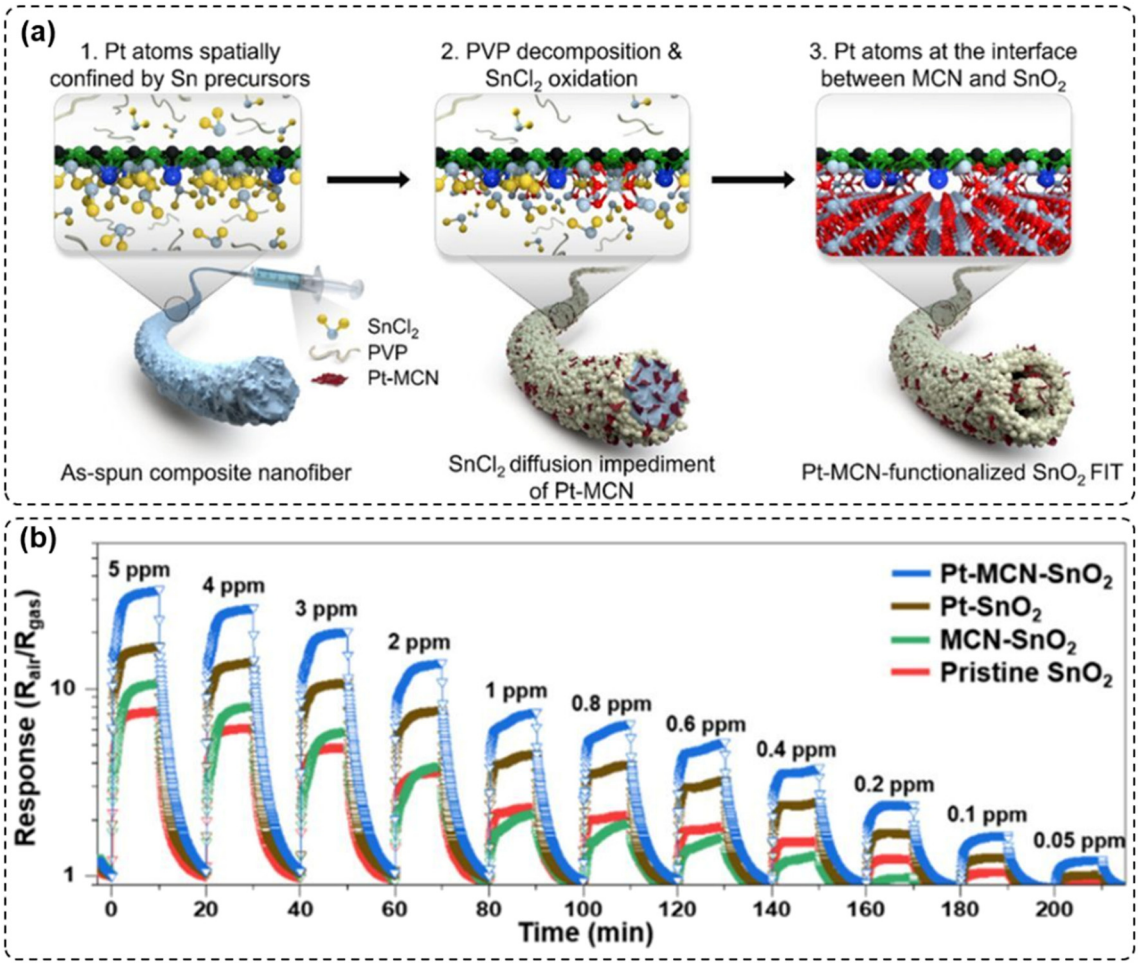

Fig. 10 (a) Schematic illustration of the Pt SA delivery process and nanofiber-in-tube structure formation. (b) Formaldehyde gas sensing results of Pt-MCN-SnO_2 compared with reference samples. Reproduced with permission.[54] Copyright 2020, American Chemical Society.

structures.[182,183] Their three-dimensionally interconnected hierarchical pores can markedly enhance gas diffusion and mass transport, allowing target molecules to rapidly penetrate the structure and fully access internal active sites, thus strengthening the response and shortening response/recovery times.[184,185] For instance, petal-like 3D hierarchical architectures can offer a larger accessible surface area and expose more defects and edge sites, increasing adsorption/reaction sites and further accelerating sensing kinetics.[186] In addition, 3D scaffolds are generally less prone to collapse or sintering during cyclic operation, leading to improved structural stability and long-term reliability.

3.5.2 Future scope of nanostructure design. Nanostructure and architecture design provide a structural foundation that governs how gas molecules, charge carriers, and reaction intermediates interact within SMO chemiresistive gas sensors. Reducing characteristic feature sizes to the nanoscale increases the fraction of surface atoms and shortens diffusion lengths for gas molecules and charge carriers. When the size of SMO nanostructures approaches or falls below the Debye length, the entire structure can become depleted or accumulated upon gas exposure, resulting in pronounced resistance modulation. This size effect enhances sensitivity by strengthening the coupling between surface reactions and bulk electrical properties, but it also renders sensor behavior more susceptible to surface states, humidity, and environmental fluctuations.

Beyond size effects, nanostructure dimensionality plays a decisive role in determining sensing behavior. 0D nanoparticles offer high surface exposure but often suffer from grain-boundary-dominated transport and poor long-term stability. 1D nanowires and nanofibers provide direct and continuous conduction pathways, enabling efficient carrier transport and reduced noise. 2D nanosheets maximize exposed surface planes and facilitate planar charge transport, while 3D hierarchical architectures integrate the advantages of multiple dimensionalities by combining high surface area with interconnected transport networks.

Porous and hollow architectures further introduce internal reaction spaces that enhance gas diffusion and accessibility to active sites. Hierarchical pore structures, consisting of micro-, meso-, and macropores, can balance gas permeability with adsorption capacity, leading to faster response and recovery kinetics. However, excessive porosity or tortuous

pore networks may hinder effective diffusion, trap reaction intermediates, or amplify humidity interference. These trade-offs underscore that porosity must be engineered with consideration of both gas flux and reaction dynamics rather than maximized indiscriminately.

Nanostructure design also critically influences charge-transport pathways and their sensitivity to surface reactions. In densely packed or randomly aggregated nanostructures, charge transport is often dominated by grain boundaries, where local potential barriers govern resistance changes. In contrast, ordered architectures with continuous conduction channels reduce the number of transport bottlenecks, enabling more predictable and stable signal transduction. Aligning nanostructure architecture with the dominant conduction pathway, whether bulk-limited or barrier-limited, is therefore essential for maximizing sensing performance.

Importantly, nanostructuring does not operate in isolation but modulates the effectiveness of other performance-enhancement strategies. Heterojunctions rely on well-defined interfaces whose impact is amplified in architectures that favor barrier-controlled transport. Defect and phase engineering benefit from nanostructures that stabilize reactive surfaces while limiting defect migration. Noble metal catalysts exhibit stronger and more uniform effects when confined within accessible and well-connected nanostructures. Similarly, filtration layers function more effectively when integrated with architectures that maintain sufficient gas flux.

From a design perspective, excessive structural complexity may compromise reproducibility, mechanical integrity, and scalability. Highly intricate architectures can introduce uncontrolled variability in pore distribution, junction density, and conduction pathways, complicating device-to-device consistency. Consequently, rational nanostructure design increasingly emphasizes simplicity, hierarchical organization, and compatibility with scalable fabrication methods rather than maximal structural novelty.

In summary, nanostructure and architecture design serve as an integrative platform that coordinates mass transport, surface chemistry, and charge transport. By aligning structural features with the dominant sensing mechanisms and complementary material strategies, nanostructuring enables balanced improvements in sensitivity, selectivity, response dynamics, and stability. When judiciously implemented, architectural design transforms individual material enhancements into coherent and reliable sensing systems suitable for practical applications.

4. Summary and outlook

Despite substantial progress in material design and device engineering, SMO chemiresistive gas sensors remain far from fully meeting the demands of real-world applications. Many of the reported performance enhancements are achieved under simplified laboratory conditions and are difficult to translate into robust, selective, and stable sensing under complex environments. From a mechanism-oriented perspective, these challenges are not incidental but are intrinsically linked to the oxygen-mediated sensing pathways and surface-dominated charge-transport characteristics of SMOs.

Improving chemical selectivity remains one of the most persistent challenges for SMO chemiresistive sensors. While strategies such as heterojunction engineering, defect regulation, and catalytic decoration can significantly amplify resistance modulation, they rarely alter the fundamental non-specific nature of oxygen-mediated surface reactions. As a result, enhanced sensitivity is often accompanied by amplified responses to interfering gases. Future progress in selectivity is expected to rely less on further amplification of surface reactivity and more on pathway-level regulation. Gas filtration, catalytic pre-conversion, and molecular sieving layers offer promising routes to decouple gas discrimination from signal transduction. In parallel, sensor arrays combined with pattern-recognition algorithms can provide system-level selectivity, although this approach introduces additional complexity and power consumption. A critical perspective shift is therefore required: selectivity should be addressed as a system design problem rather than a single-material optimization task.

Humidity interference represents a fundamental limitation for most SMO-based sensors due to the strong interaction between water molecules and oxide surfaces. As discussed earlier, water adsorption does not merely compete with target gases but can modify surface reaction pathways, charge-carrier distribution, and baseline resistance. Many reported sensing mechanisms implicitly assume dry conditions, leading to discrepancies between laboratory performance and field operation. Addressing humidity effects requires integrating hydrophobic surface modification, humidity-tolerant filtration layers, and stable defect or phase configurations that minimize water-induced reconstruction. Importantly, humidity tolerance should be evaluated under realistic operating conditions and over extended time scales. Treating humidity as an external variable rather than an intrinsic design constraint risks overestimating sensor reliability and applicability.

Long-term stability and reproducibility remain critical bottlenecks for SMO chemiresistive sensors, particularly those relying on aggressive defect engineering, metastable phases, or highly dispersed noble metal species. Defect migration, phase transformation, catalyst aggregation, and surface contamination can all lead to baseline drift and performance degradation. Future research should place greater emphasis on stabilized material configurations, such as defect states anchored by strong local coordination, phase boundaries with thermodynamic robustness, and noble metal species confined within well-defined architectures. Equally important is the establishment of standardized testing protocols that assess stability under cyclic operation, varying humidity, and mixed-gas environments. Without such benchmarks, it remains difficult to compare reported results or assess practical viability.

At present, most chemiresistive gas sensors operate with air as the default background, and their sensing mechanisms and

material systems are typically designed and optimized for the gas composition and concentration ranges encountered in ambient atmospheres. However, as application scenarios continue to expand and performance requirements become more stringent, these sensors will increasingly face environments that are more complex and more extreme. This shift imposes higher demands on sensitivity, selectivity, long-term stability, and overall environmental adaptability. For instance, during the transportation and storage of special gases, such as flammable, explosive, toxic, or high-purity industrial gases, real-time and accurate monitoring of sealing integrity in closed systems is often required. Such environments may feature a highly simplified background composition, elevated pressure or concentration, and in some cases little to no oxygen, which differs fundamentally from an air background. Consequently, sensors must deliver reliable and repeatable responses under oxygen-deficient or oxygen-free conditions. Moreover, emerging needs in aerospace, semiconductor manufacturing, and vacuum metallurgy call for trace and complex gas detection under vacuum or near-vacuum backgrounds. Under these extreme conditions, gas transport, surface adsorption/reaction kinetics, and thermal management can change substantially, meaning that sensing models and calibration protocols developed for air-based operation may no longer be valid. Therefore, to enable future deployment in complex and extreme environments, chemiresistive gas sensors require systematic innovation across materials, structures, operating modes, and signal processing. Promising directions include developing sensing materials and interfacial architectures compatible with wide pressure ranges and low-oxygen atmospheres, establishing robust sensing mechanisms for oxygen-free or vacuum conditions, improving resistance to interference and drift, and enhancing robustness through approaches such as temperature modulation, pulsed operation, and algorithm-assisted signal decoupling. These advances are essential for achieving accurate and reliable detection across diverse operating regimes.

Conflicts of interest

The authors declare no conflict of interest.

Data availability

No primary research data were generated as part of this review. All information supporting the conclusions of this work was obtained from previously published studies, which have been appropriately cited.

Acknowledgements

The authors acknowledge the financial support from the National Natural Science Foundation of China (52322312, 51973227, 22005011, 21633014, 51901009 and 21988102), the Fundamental Research Funds for the Central Universities and Jilin Provincial Natural Science Foundation (YDZJ202601ZYTS110).

References

1 P. Kortoçi, N. H. Motlagh, M. A. Zaidan, P. L. Fung, S. Varjonen, A. Rebeiro-Hargrave, J. V. Niemi, P. Nurmi, T. Hussein, T. Petäjä, M. Kulmala and S. Tarkoma, *Smart Health*, 2022, **23**, 100241.
2 K. Sivaperuman, A. Thomas, R. Thangavel, L. Thirumalaisamy, S. Palanivel, S. Pitchaimuthu, N. Ahsan and Y. Okada, *Prog. Mater. Sci.*, 2024, **142**, 101222.
3 H. G. Birnbaum, C. D. Carley, U. Desai, S. Ou and P. R. Zuckerman, *Health Aff.*, 2020, **39**, 2113.
4 S. Chen, J. J. M. Vequizo, Z. Pan, T. Hisatomi, M. Nakabayashi, L. Lin, Z. Wang, K. Kato, A. Yamakata, N. Shibata, T. Takata, T. Yamada and K. Domen, *J. Am. Chem. Soc.*, 2021, **143**, 10633.
5 C. Hu, W. Zhang, J. Yang, Y. Pei, X. Tan, B. Dong, H. Song and L. Xu, *Chem. Soc. Rev.*, 2025, **54**, 11302.
6 Z. U. Abideen, J.-H. Kim, J.-H. Lee, J.-Y. Kim, A. Mirzaei, H. W. Kim and S. S. Kim, *J. Korean Ceram. Soc.*, 2017, **54**, 366.
7 J. Hu, Y. Zou, Y. Deng, H.-J. Li, H. Xu, D. Wang, L. Wu, Y. Deng and G. Li, *Prog. Mater. Sci.*, 2025, **150**, 101409.
8 L. Zhang, M. Zhou, F. Meng, J. Bai, D. Wang, M. Tang and Z. Wu, *TrAC, Trends Anal. Chem.*, 2025, **187**, 118213.
9 J. Li, H. Zhao, Y. Wang and Y. Zhou, *Sens. Diagn.*, 2024, **3**, 336.
10 J. Cai, C. Zhang, A. Khan, C. Liang and W. D. Li, *RSC Adv.*, 2018, **8**, 5312.
11 W. Li, M. J. Lefferts, Y. Wang, A. M. Lister, A. Forssberg, R. Chen, L. Wang and M. R. Castell, *Adv. Mater. Interfaces*, 2023, **10**, 2202042.
12 M. Kamalabadi, A. Ghoorchian, K. Derakhshandeh, M. Gholyaf and M. Ravan, *Anal. Chem.*, 2022, **94**, 16290.
13 T. Y. Yu, Q. Niu, Y. Chen, M. Lu, M. Zhang, J. W. Shi, J. Liu, Y. Yan, S. L. Li and Y. Q. Lan, *J. Am. Chem. Soc.*, 2023, **145**, 8860.
14 S. Wang, Q. Fan, L. Wang, X. Ma, F. Gao, L. Du and Q. H. Zhao, *Angew. Chem., Int. Ed.*, 2025, **64**, e202518302.
15 Y.-J. Chen, Y.-M. Xu, X.-L. Ye, Z.-P. Luo, S.-P. Zhu, K.-F. Li, J.-F. Lu, G.-E. Wang and G. Xu, *Nat. Commun.*, 2025, **16**, 6634.
16 S. Lee, T. Y. Ko, A. K. Jena, H. Kang, J. Jeon, W. Yang, S. H. Kim, H. T. Jung, S. C. Lee and S. J. Kim, *Small*, 2025, **21**, e08501.
17 L. Xu, H. Liu, Q. Song, X. Sun, Z. Zhao, Z. Ge, Y. Chen, X. Jiang and L. Jiang, *Mater. Horiz.*, 2025, **12**, 10091.
18 B. Lei, H. Zhang, Q. Zhao, W. Liu, Y. Wei, Y. Lu, T. Xiao, J. Kong and W. Cai, *Nanomaterials*, 2023, **13**, 733.
19 D. Fu, C. Zhu, X. Zhang, C. Li and Y. Chen, *J. Mater. Chem. A*, 2016, **4**, 1390.
20 X. Song, Q. Xu, T. Zhang, B. Song, C. Li and B. Cao, *Sens. Actuators, B*, 2018, **268**, 170.
21 D. Zhang, J. Jiang, T. Wang, F. Li, H. Yu, X. Dong and Y. Yang, *Sens. Actuators, B*, 2024, **421**, 136543.

22 T. Dutta, T. Noushin, S. Tabassum and S. K. Mishra, *Sensors*, 2023, **23**, 6849.
23 P. Wang, S. Xu, X. Shi, J. Zhu, H. Xiong and H. Wen, *Chemosensors*, 2025, **13**, 224.
24 P. Najafi and A. Ghaemi, *Chem. Eng. J.*, 2024, **498**, 154999.
25 H. Mei, J. Peng, T. Wang, T. Zhou, H. Zhao, T. Zhang and Z. Yang, *Nano-Micro Lett.*, 2024, **16**, 269.
26 H. Chai, Z. Zheng, K. Liu, J. Xu, K. Wu, Y. Luo, H. Liao, M. Debliquy and C. Zhang, *IEEE Sens. J.*, 2022, **22**, 5470.
27 F. J. Meng, R. F. Xin and S. X. Li, *Materials*, 2022, **16**, 263.
28 A. Staerz, U. Weimar and N. Barsan, *Sens. Actuators, B*, 2022, **358**, 131531.
29 N. Yamazoe and K. Shimanoe, *Sens. Actuators, B*, 2008, **128**, 566.
30 N. Barsan, C. Simion, T. Heine, S. Pokhrel and U. Weimar, *J. Electroceram.*, 2009, **25**, 11.
31 M. E. Franke, T. J. Koplin and U. Simon, *Small*, 2006, **2**, 36.
32 A. Kumar, J. T. Mazumder, K. Joyen, F. Favier, A. Mirzaei, J.-Y. Kim, M. Kwoka, M. Bechelany, R. K. Jha, M. Kumar, H. W. Kim and S. S. Kim, *Coord. Chem. Rev.*, 2025, **541**, 216836.
33 H.-J. Kim and J.-H. Lee, *Sens. Actuators, B*, 2014, **192**, 607.
34 P. M. Bulemo, D.-H. Kim, H. Shin, H.-J. Cho, W.-T. Koo, S.-J. Choi, C. Park, J. Ahn, A. T. Güntner, R. M. Penner and I.-D. Kim, *Chem. Rev.*, 2025, **125**, 4111.
35 E. Ciftyurek, Z. Li and K. Schierbaum, *Sensors*, 2022, **23**, 29.
36 A. Kumar, S. S. Kim, H. W. Kim and M. Kumar, *Nano Express*, 2023, **4**, 042003.
37 S. Kucharski, M. Vorochta, L. Piliai, A. M. Beale and C. Blackman, *ACS Sens.*, 2025, **10**, 1898.
38 C. Yuan, J. Ma, Y. Zou, G. Li, H. Xu, V. V. Sysoev, X. Cheng and Y. Deng, *Adv. Sci.*, 2022, **9**, 2203594.
39 Y. Xiong, Y. Lin, X. Wang, Y. Zhao and J. Tian, *Adv. Powder Mater.*, 2022, **1**, 100033.
40 C. Ding, Y. Ma, X. Lai, Q. Yang, P. Xue, F. Hu and W. Geng, *ACS Appl. Mater. Interfaces*, 2017, **9**, 18170.
41 Y. F. Sun, S. B. Liu, F. L. Meng, J. Y. Liu, Z. Jin, L. T. Kong and J. H. Liu, *Sensors*, 2012, **12**, 2610.
42 M. Al-Hashem, S. Akbar and P. Morris, *Sens. Actuators, B*, 2019, **301**, 126845.
43 M. Hübner, C. E. Simion, A. Tomescu-Stănoiu, S. Pokhrel, N. Bârsan and U. Weimar, *Sens. Actuators, B*, 2011, **153**, 347.
44 Y. Wang and Y. Zhou, *Materials*, 2022, **15**, 8728.
45 I. Boehme, U. Weimar and N. Barsan, *Sens. Actuators, B*, 2021, **326**, 129004.
46 G. Korotcenkov and B. K. Cho, *Sens. Actuators, B*, 2013, **188**, 709.
47 S. Dong, D. Wu, W. Gao, H. Hao, G. Liu and S. Yan, *Dalton Trans.*, 2020, **49**, 1300.
48 L. Huo, X. Yang, Z. Liu, X. Tian, T. Qi, X. Wang, K. Yu, J. Sun and M. Fan, *Sens. Actuators, B*, 2017, **244**, 694.
49 D.-X. Ju, H.-Y. Xu, Z.-W. Qiu, Z.-C. Zhang, Q. Xu, J. Zhang, J.-Q. Wang and B.-Q. Cao, *ACS Appl. Mater. Interfaces*, 2015, **7**, 19163.
50 F. Li, B. Yang, J. Li, Y. Long, Z. Zhang, Z. Wang, J. Wang, G. Chen, Z. Zhang, R. Yang, K. Wang, W. Zou, F. Fang, Y. Zhang, P. Wang and Z. Zhan, *ACS Sens.*, 2025, **10**, 6971.
51 J. M. Suh, W. Sohn, Y.-S. Shim, J.-S. Choi, Y. G. Song, T. L. Kim, J.-M. Jeon, K. C. Kwon, K. S. Choi, C.-Y. Kang, H.-G. Byun and H. W. Jang, *ACS Appl. Mater. Interfaces*, 2017, **10**, 1050.
52 Y. J. Kwon, S. Y. Kang, P. Wu, Y. Peng, S. S. Kim and H. W. Kim, *ACS Appl. Mater. Interfaces*, 2016, **8**, 13646.
53 H. I. Ahemad, M. A. More, P. Hiremath, N. Naik, S. D. Shinde, D. Y. Patil, D. D. Kajale, G. H. Jain, J. M. Kim, R. N. Bulakhe and G. E. Patil, *Small*, 2025, **21**, e05604.
54 H. Shin, W.-G. Jung, D.-H. Kim, J.-S. Jang, Y. H. Kim, W.-T. Koo, J. Bae, C. Park, S.-H. Cho, B. J. Kim and I.-D. Kim, *ACS Nano*, 2020, **14**, 11394.
55 H. Shin, J. Ko, C. Park, D. H. Kim, J. Ahn, J. S. Jang, Y. H. Kim, S. H. Cho, H. Baik and I. D. Kim, *Adv. Funct. Mater.*, 2022, **32**, 2110485.
56 S.-Y. Jeong, Y. K. Moon, J. Wang and J.-H. Lee, *Nat. Commun.*, 2023, **14**, 233.
57 P. Wu, Y. Li, Y. Luo, Y. Yan, R. Zhuo, D. Wang, J. Tang, H. Yuan, X. Zhang and S. Xiao, *Adv. Funct. Mater.*, 2025, **35**, 2415517.
58 J. Hu, X. Xiong, W. Guan, H. Long, L. Zhang and H. Wang, *Sens. Actuators, B*, 2022, **361**, 131705.
59 J. S. Jang, S. E. Lee, S. J. Choi, W. T. Koo, D. H. Kim, H. Shin, H. J. Park and I. D. Kim, *Adv. Funct. Mater.*, 2019, **29**, 1903012.
60 S. Ippolito, A. G. Kelly, R. Furlan de Oliveira, M.-A. Stoeckel, D. Iglesias, A. Roy, C. Downing, Z. Bian, L. Lombardi, Y. A. Samad, V. Nicolosi, A. C. Ferrari, J. N. Coleman and P. Samorì, *Nat. Nanotechnol.*, 2021, **16**, 592.
61 S. Wei, S. Li, R. Wei, S. Liu and W. Du, *Sens. Actuators, B*, 2021, **329**, 129188.
62 A. Turlybekuly, Y. Shynybekov, B. Soltabayev, G. Yergaliuly and A. Mentbayeva, *ACS Sens.*, 2024, **9**, 6358.
63 S. Ji, Y. Chen, X. Wang, Z. Zhang, D. Wang and Y. Li, *Chem. Rev.*, 2020, **120**, 11900.
64 S. Y. Jeong, Y. K. Moon, T. H. Kim, S. W. Park, K. B. Kim, Y. C. Kang and J. H. Lee, *Adv. Sci.*, 2020, **7**, 1903093.
65 J. van den Broek, A. T. Güntner and S. E. Pratsinis, *ACS Sens.*, 2018, **3**, 677.
66 A. Shanmugasundaram, N. D. Chinh, Y.-J. Jeong, T. F. Hou, D.-S. Kim, D. Kim, Y.-B. Kim and D.-W. Lee, *J. Mater. Chem. A*, 2019, **7**, 9263.
67 Y. Kim, Y. S. Choi, S. Y. Park, T. Kim, S.-P. Hong, T. H. Lee, C. W. Moon, J.-H. Lee, D. Lee, B. H. Hong and H. W. Jang, *Nanoscale*, 2019, **11**, 2966.
68 S. Y. Jeong, J. S. Kim and J. H. Lee, *Adv. Mater.*, 2020, **32**, e2002075.
69 L. Liu, Y. Wang, Y. Liu, S. Wang, T. Li, S. Feng, S. Qin and T. Zhang, *Microsyst. Nanoeng.*, 2022, **8**, 85.
70 S. Yang, G. Lei, H. Xu, Z. Lan, Z. Wang and H. Gu, *Nanomaterials*, 2021, **11**, 1026.
71 X. He, H. Chai, Y. Luo, L. Min, M. Debliquy and C. Zhang, *J. Adv. Ceram.*, 2023, **12**, 207.

72 T. T. Nga Phan, T. T. My Dinh, M. Duc Nguyen, L. Dan, C. Nhan Phan, T. Kien Pham, C. Tu Nguyen and T. Huyen Pham, *Sens. Actuators, B*, 2022, **354**, 131195.
73 G. Korotcenkov, *Mater. Sci. Eng., B*, 2007, **139**, 1.
74 T. Zhou and T. Zhang, *Small Methods*, 2021, **5**, 2100515.
75 L. Xu, M. Ge, F. Zhang, H. Huang, Y. Sun and D. He, *J. Mater. Res.*, 2020, **35**, 3079.
76 R. Vishnuraj, K. K. Karuppanan, M. Aleem and B. Pullithadathil, *Nanoscale Adv.*, 2020, **2**, 4785.
77 S. Zhu, H. Fan, Y. Jia, Y. Fan and W. Wang, *J. Mater. Chem. A*, 2025, **13**, 32665.
78 J. Wang, Y. Chen, Y. Shen, S. Liu and Y. Zhang, *Chem. Commun.*, 2017, **53**, 2978.
79 Y. Fan, L. Li, B. Song, H. Wu, L. Qi, M. Khan, H. Wu and K. Shi, *Sens. Actuators, B*, 2024, **404**, 135299.
80 T. Lin, X. Lv, Z. Hu, A. Xu and C. Feng, *Sensors*, 2019, **19**, 233.
81 A. Marikutsa, M. Rumyantseva, E. A. Konstantinova and A. Gaskov, *Sensors*, 2021, **21**, 2554.
82 W. Ding, D. Liu, J. Liu and J. Zhang, *Chin. J. Chem.*, 2020, **38**, 1832.
83 R. S. Ganesh, E. Durgadevi, M. Navaneethan, V. L. Patil, S. Ponnusamy, C. Muthamizhchelvan, S. Kawasaki, P. S. Patil and Y. Hayakawa, *Sens. Actuators, A*, 2018, **269**, 331.
84 T. Wang, Q. Xing, R. Zhai, T. Huang and P. Song, *ACS Sens.*, 2024, **9**, 3178.
85 F. Lei, Y. Sun, K. Liu, S. Gao, L. Liang, B. Pan and Y. Xie, *J. Am. Chem. Soc.*, 2014, **136**, 6826.
86 M. Setvín, M. Wagner, M. Schmid, G. S. Parkinson and U. Diebold, *Chem. Soc. Rev.*, 2017, **46**, 1772.
87 R. Merkle and J. Maier, *Angew. Chem., Int. Ed.*, 2008, **47**, 3874.
88 H. Y. Xu, Y. H. Huang, S. Liu, K. W. Xu, F. Ma and P. K. Chu, *RSC Adv.*, 2016, **6**, 79383.
89 M. Sakamoto, R. Fujita, M. Nishikawa, H. Hirazawa, Y. Ueno, M. Yamamoto and S. Takaoka, *Materials*, 2024, **17**, 395.
90 C. Brooks and S. Lany, *npj Comput. Mater.*, 2025, **11**, 339.
91 G. Müller and G. Sberveglieri, *Chemosensors*, 2022, **10**, 171.
92 J. Pan, Y. Li, Z. Yang and D. A. Hall, *J. Eur. Ceram. Soc.*, 2024, **44**, 2095.
93 R. Papšík, O. Ševeček, J. Schlacher and R. Bermejo, *Eng. Fract. Mech.*, 2024, **303**, 110121.
94 Y. Yuan, Y. Wang, M. Wang, J. Liu, C. Pei, B. Liu, H. Zhao, S. Liu and H. Yang, *Sci. Rep.*, 2017, **7**, 1231.
95 S. Somacescu, C. Ghica, C. E. Simion, A. C. Kuncser, A. M. Vlaicu, M. Stefan, D. Ghica, O. G. Florea, I. F. Mercioniu and A. Stanoiu, *Sens. Actuators, B*, 2019, **294**, 148.
96 Y. Li, B. Zu, Y. Guo, K. Li, H. Zeng and X. Dou, *Small*, 2016, **12**, 1420.
97 S. Deepa, K. Prasanna Kumari and B. Thomas, *Ceram. Int.*, 2017, **43**, 17128.
98 J. Lee, M. Kim, S. Park, J. Ahn and I. D. Kim, *Adv. Mater.*, 2025, **37**, e08204.
99 X. Gao and T. Zhang, *Sens. Actuators, B*, 2018, **277**, 604.
100 Y. Liang, Y. Yang, H. Zhou, C. Zou, K. Xu, X. Luo, T. Yu, W. Zhang, Y. Liu and C. Yuan, *Ceram. Int.*, 2019, **45**, 6282.
101 S. Singh, K. Y. Shin, S. Moon, S. S. Kim and H. W. Kim, *ACS Sens.*, 2024, **9**, 3994.
102 A. K. Gangwar, R. Godiwal, U. Varshney, S. Das, J. S. Tawale, G. Gupta and P. Singh, *Appl. Surf. Sci.*, 2024, **655**, 159607.
103 K. Zakrzewska and M. Radecka, *Nanoscale Res. Lett.*, 2017, **12**, 89.
104 X. Li, L. Fu, H. Karimi-Maleh, F. Chen and S. Zhao, *Heliyon*, 2024, **10**, e27740.
105 M. S. Yao, W. X. Tang, G. E. Wang, B. Nath and G. Xu, *Adv. Mater.*, 2016, **28**, 5229.
106 X. He, P. Guo, X. An, Y. Li, J. Chen, X. Zhang, L. Wang, M. Dai, C. Tan and J. Zhang, *Int. J. Extreme Manuf.*, 2024, **6**, 032007.
107 T. Chu, C. Rong, L. Zhou, X. Mao, B. Zhang and F. Xuan, *Adv. Mater.*, 2023, **35**, 2206783.
108 B. Feng, Z. Wang, Y. Feng, P. Li, Y. Zhu, Y. Deng, L. Wu, Q. Yue and J. Wei, *ACS Nano*, 2024, **18**, 22888.
109 G. Lei, H. Pan, H. Mei, X. Liu, G. Lu, C. Lou, Z. Li and J. Zhang, *Chem. Soc. Rev.*, 2022, **51**, 7260.
110 Y. Qian, G. Zhao, C. Zhang, S. Yin, J. Chen, Y. Luo, Z. Huang, B. Liu and G. Duan, *Commun. Mater.*, 2025, **6**, 137.
111 Y. Yu, Y. Tan, W. Niu, S. Zhao, J. Hao, Y. Shi, Y. Dong, H. Liu, C. Huang, C. Gao, P. Zhang, Y. Wu, L. Zeng, B. Du and Y. He, *Materials*, 2024, **17**, 1970.
112 Y. Xu, W. Zheng, X. Liu, L. Zhang, L. Zheng, C. Yang, N. Pinna and J. Zhang, *Mater. Horiz.*, 2020, **7**, 1519.
113 S. Chae, Y. Chen, J. Yang and J. Su, *Surf. Sci. Technol.*, 2024, **2**, 18.
114 S. Liu, J. Li and H. Xiong, *Front. Chem.*, 2022, **10**, 959525.
115 C. Rong, K. Flint, C. Doonan and Y. Chen, *Next Mater.*, 2025, **7**, 100457.
116 D. Cai, J. Zhang, Z. Kong and Z. Li, *ChemCatChem*, 2024, **16**, e202301414.
117 Y. Liang, C. Wu, S. Meng, Z. Lu, R. Zhao, H. Wang, Z. Liu and J. Wang, *ACS Appl. Mater. Interfaces*, 2023, **15**, 30262.
118 Z. Zhang, C. Feng, C. Liu, M. Zuo, L. Qin, X. Yan, Y. Xing, H. Li, R. Si, S. Zhou and J. Zeng, *Nat. Commun.*, 2020, **11**, 1215.
119 S. Chen and P. Liu, *Mater. Chem. Front.*, 2024, **8**, 1334.
120 B. J. O'Neill, D. H. K. Jackson, J. Lee, C. Canlas, P. C. Stair, C. L. Marshall, J. W. Elam, T. F. Kuech, J. A. Dumesic and G. W. Huber, *ACS Catal.*, 2015, **5**, 1804.
121 Z. Wang, Y. Zhang, E. C. Neyts, X. Cao, X. Zhang, B. W. L. Jang and C.-j. Liu, *ACS Catal.*, 2018, **8**, 2093.
122 D. Degler, U. Weimar and N. Barsan, *ACS Sens.*, 2019, **4**, 2228.
123 P. He, H. Fu, X. Yang, S. Xiong and X. An, *Sens. Actuators, B*, 2022, **362**, 131760.
124 B. Ni and X. Wang, *Adv. Sci.*, 2015, **2**, 1500085.
125 M. P. C. van Etten, B. Zijlstra, E. J. M. Hensen and I. A. W. Filot, *ACS Catal.*, 2021, **11**, 8484.
126 R. Yao, Y. Xia, L. Yang, J. Xiang, Q. Zhao and S. Guo, *Molecules*, 2025, **30**, 4683.
127 C. Wang, L. Yin, L. Zhang, D. Xiang and R. Gao, *Sensors*, 2010, **10**, 2088.

128 J. Yan and Z. Song, *J. Alloys Compd.*, 2024, **976**, 173075.
129 D. Leybo, U. J. Etim, M. Monai, S. R. Bare, Z. Zhong and C. Vogt, *Chem. Soc. Rev.*, 2024, **53**, 10450.
130 Y. Xia, Y. Xiong, B. Lim and S. E. Skrabalak, *Angew. Chem., Int. Ed.*, 2009, **48**, 60.
131 P. Zou, Z. Ma, Z. Tang, X. Gao, X. Hou and L. Jia, *ACS ES&T Eng.*, 2025, **5**, 260.
132 V. Palmisano, E. Weidner, L. Boon-Brett, C. Bonato, F. Harskamp, P. Moretto, M. B. Post, R. Burgess, C. Rivkin and W. J. Buttner, *Int. J. Hydrogen Energy*, 2015, **40**, 11740.
133 C. T. Campbell, *Acc. Chem. Res.*, 2013, **46**, 1712.
134 X. Han and S. Yang, *Chem*, 2022, **8**, 2571.
135 J. Liu, H. Xu, J. Zhu and D. Cheng, *JACS Au*, 2023, **3**, 3031.
136 A. Alvarez-Garcia, L. M. Molina and I. L. Garzon, *Phys. Chem. Chem. Phys.*, 2024, **26**, 15902.
137 J. van den Broek, I. C. Weber, A. T. Güntner and S. E. Pratsinis, *Mater. Horiz.*, 2021, **8**, 661.
138 A. T. Güntner, S. Abegg, K. Wegner and S. E. Pratsinis, *Sens. Actuators, B*, 2018, **257**, 916.
139 X. Xiaowen, W. Jing and L. Yingcai, *Sensors*, 2006, **6**, 1751.
140 J.-S. Jang, L. R. Winter, C. Kim, J. D. Fortner and M. Elimelech, *Trends Chem.*, 2021, **3**, 547.
141 S. Freddi, C. Marzuoli, S. Pagliara, G. Drera and L. Sangaletti, *RSC Adv.*, 2022, **13**, 251.
142 H. G. Girma, K. H. Park, D. Ji, Y. Kim, H. M. Lee, S. Jeon, S. H. Jung, J. Y. Kim, Y. Y. Noh and B. Lim, *Adv. Funct. Mater.*, 2023, **33**, 2213381.
143 G. Liu, V. Chernikova, Y. Liu, K. Zhang, Y. Belmabkhout, O. Shekhah, C. Zhang, S. Yi, M. Eddaoudi and W. J. Koros, *Nat. Mater.*, 2018, **17**, 283.
144 Z. Yang, A. Mei, W. Chen, Z. Wang, H. Guo and Y. Liu, *Sens. Actuators, B*, 2023, **392**, 134051.
145 K. Hwang, J. Ahn, I. Cho, K. Kang, K. Kim, J. Choi, K. Polychronopoulou and I. Park, *ACS Appl. Mater. Interfaces*, 2020, **12**, 13338.
146 Y. Zheng, X. Li and P. K. Dutta, *Sensors*, 2012, **12**, 5170.
147 Z. Cao, N. Anjikar and S. Yang, *Separations*, 2022, **9**, 47.
148 A. Fernandez-Barquin, R. Rea, D. Venturi, M. Giacinti-Baschetti, M. G. De Angelis, C. Casado-Coterillo and A. Irabien, *RSC Adv.*, 2018, **8**, 3536.
149 P. Tarttelin Hernández, S. M. V. Hailes and I. P. Parkin, *Sens. Actuators, B*, 2017, **242**, 1281.
150 M. Sakai, Y. Koshiishi, A. Okada, K. Kawanishi, K. Masuda and M. Matsukata, *Cryst. Growth Des.*, 2025, **25**, 5584.
151 X. Wu, S. Xiong, Z. Mao, S. Hu and X. Long, *Chemistry*, 2017, **23**, 7969.
152 A. Huang, Q. Liu, N. Wang, Y. Zhu and J. Caro, *J. Am. Chem. Soc.*, 2014, **136**, 14686.
153 J. Shen, G. Liu, K. Huang, Z. Chu, W. Jin and N. Xu, *ACS Nano*, 2016, **10**, 3398.
154 Y. Jin, Y. Fan, X. Meng, W. Zhang, B. Meng, N. Yang and S. Liu, *Processes*, 2019, **7**, 751.
155 K. Seehamart, W. Busayaporn and R. Chanajaree, *RSC Adv.*, 2023, **13**, 19207.
156 A. W. Ameen, P. M. Budd and P. Gorgojo, *Membranes*, 2020, **10**, 413.
157 K. Ramezani Shabolaghi and M. Irani, *Comput. Theor. Chem.*, 2022, **1207**, 113498.
158 C. Chuah, J. Lee and T.-H. Bae, *Membranes*, 2020, **10**, 336.
159 H. Hu, J. Zhu, F. Yang, Z. Chen, M. Deng, L. Weng, Y. Ling and Y. Zhou, *Chem. Commun.*, 2019, **55**, 6495.
160 G. Golemme and A. Santaniello, *Membranes*, 2019, **9**, 19.
161 I. C. Weber, H. P. Braun, F. Krumeich, A. T. Güntner and S. E. Pratsinis, *Adv. Sci.*, 2020, **7**, 2001503.
162 F. Maximilian, K. Susanne, W. Thomas, F. Joachim and H. Meixner, *Sens. Actuators, B*, 2000, **69**, 205.
163 L. Xue, J. Cui, R. Li, W. Xie, K. Chen, H. Yu, L. Wu, T. Ni, Q. Yue and Y. Deng, *Adv. Mater.*, 2025, **37**, 2416006.
164 I. C. Weber and A. T. Güntner, *Sens. Actuators, B*, 2022, **356**, 131346.
165 R. Qin, Q. Yuan, J. Yu, J. Hu, W. Zhang, Y. Wang, Y. Cao, Q. Ma, S. Li, G. Li and D. Wang, *ACS Appl. Mater. Interfaces*, 2025, **17**, 16920.
166 G. Jiménez-Cadena, J. Riu and F. X. Rius, *Analyst*, 2007, **132**, 1083.
167 Z. Li, H. Li, Z. Wu, M. Wang, J. Luo, H. Torun, P. Hu, C. Yang, M. Grundmann, X. Liu and Y. Fu, *Mater. Horiz.*, 2019, **6**, 470.
168 A. Mirzaei, H. R. Ansari, M. Shahbaz, J.-Y. Kim, H. W. Kim and S. S. Kim, *Chemosensors*, 2022, **10**, 289.
169 Paras, K. Yadav, P. Kumar, D. R. Teja, S. Chakraborty, M. Chakraborty, S. S. Mohapatra, A. Sahoo, M. M. C. Chou, C.-T. Liang and D.-R. Hang, *Nanomaterials*, 2022, **13**, 160.
170 X. Chaonan, T. Jun, M. Norio and Y. Noboru, *Sens. Actuators, B*, 1991, **3**, 147.
171 N. K. Chowdhury and B. Bhowmik, *Nanoscale Adv.*, 2021, **3**, 73.
172 V. Galstyan, *Anal. Chim. Acta*, 2021, **1152**, 238192.
173 N. Chakraborty, A. Sanyal, S. Das, D. Saha, S. K. Medda and S. Mondal, *ACS Appl. Nano Mater.*, 2020, **3**, 7572.
174 W. Zhang, B. Yang, J. Liu, X. Chen, X. Wang and C. Yang, *Sens. Actuators, B*, 2017, **243**, 982.
175 M. M. Arafat, B. Dinan, S. A. Akbar and A. S. Haseeb, *Sensors*, 2012, **12**, 7207.
176 P. Karnati, S. Akbar and P. A. Morris, *Sens. Actuators, B*, 2019, **295**, 127.
177 F. Li, X. Gao, R. Wang, T. Zhang, G. Lu and N. Barsan, *ACS Appl. Mater. Interfaces*, 2016, **8**, 19799.
178 M. Donarelli and L. Ottaviano, *Sensors*, 2018, **18**, 3638.
179 S. Yang, C. Jiang and S.-h. Wei, *Appl. Phys. Rev.*, 2017, **4**, 021304.
180 T. Li, W. Yin, S. Gao, Y. Sun, P. Xu, S. Wu, H. Kong, G. Yang and G. Wei, *Nanomaterials*, 2022, **12**, 982.
181 M. N. Norizan, N. Abdullah, N. A. Halim, S. Z. N. Demon and I. S. Mohamad, *Nanomaterials*, 2022, **12**, 2278.
182 Y. Liu, S. Xiao and K. Du, *Adv. Mater. Interfaces*, 2021, **8**, 2002122.
183 H. Yu, C. Guo, X. Zhang, Y. Xu, X. Cheng, S. Gao and L. Huo, *Adv. Sustainable Syst.*, 2022, **6**, 2100370.
184 J.-H. Lee, *Sens. Actuators, B*, 2009, **140**, 319.

185 Y. Qin, F. Zhang, Y. Chen, Y. Zhou, J. Li, A. Zhu, Y. Luo, Y. Tian and J. Yang, *J. Phys. Chem. C*, 2012, **116**, 11994.

186 C. Liu, B. Wang, T. Liu, P. Sun, Y. Gao, F. Liu and G. Lu, *Sens. Actuators, B*, 2016, **235**, 294.